

# Solvable entanglement dynamics in quantum circuits with generalized dual unitarity

Chuan Liu<sup>1,\*</sup> and Wen Wei Ho<sup>1,2,†</sup>

<sup>1</sup>*Department of Physics, National University of Singapore, Singapore 117542*

<sup>2</sup>*Centre for Quantum Technologies, National University of Singapore, 3 Science Drive 2, Singapore 117543*

(Dated: December 20, 2023)

We study the non-equilibrium dynamics of kicked Ising models in  $1+1$  dimensions which have interactions alternating between odd and even bonds in time. These models give rise to time-evolution equivalent to quantum circuits having both the global property of tri-unitarity (three ‘arrows of time’) and also the local property of second-level dual-unitarity, which constrains the behavior of pairs of local gates underlying the circuit under a space-time rotation. We identify a broad class of initial product states wherein the effect of the environment on a small subsystem can be exactly represented by influence matrices with simple Markovian structures, resulting in the subsystem’s full dynamics being efficiently computable. We further find additional conditions under which the dynamics of entanglement can be solved for all times, yielding rich phenomenology ranging from linear growth at half the maximal speed allowed by locality, followed by saturation to maximum entropy (i.e., thermalization to infinite temperature); to entanglement growth with saturation to extensive but sub-maximal entropy. Our findings extend our knowledge of interacting quantum systems whose thermalizing dynamics can be efficiently and analytically computed, going beyond the well-known examples of integrable models, Clifford circuits, and dual-unitary circuits.

*Introduction.*—Understanding the dynamics of nonequilibrium quantum many-body systems is one of the central challenges in modern physics: it finds relevance in diverse topics ranging from thermalization in condensed matter and statistical mechanics [1–4], to operator spreading and information scrambling of black holes in high-energy physics [5–10]. Dynamics in the far-from-equilibrium regime though is typically difficult to describe. This is due to the large build-up over time of entanglement between different spatial regions, resulting in exponentially many quantum correlations that need to be tracked. Exact classical simulations are therefore limited to small system sizes, while approximate analytic and numerical methods like mean-field theory [11] and matrix product states (MPS) [12–15] can deal with large sizes but quickly lose validity at late times. Solvable models of interacting quantum dynamics are thus highly valuable. However, these are far and few between. Current known examples include integrable systems [16–19], Clifford circuits [20–23], as well as the recently introduced class of dual-unitary quantum circuits [24–28], characterized by unitarity of local gates in both space and time directions. Dual-unitary dynamics is particularly interesting, as it is rich enough to exhibit quantum chaos [24, 29], a feature expected of generic interacting quantum dynamics.

In this Letter, we study non-equilibrium dynamics of kicked Ising models acting on 1D chains of qudits, with interactions alternating between odd and even bonds in time. These models’ dynamics can equivalently be understood as arising from quantum circuits going beyond dual-unitarity, as they have a global property of tri-unitarity [30] (having three ‘arrows of time’), and can be built up from two-local gates possessing a so-called ‘second level dual unitary’ (2DU) property, a concept re-

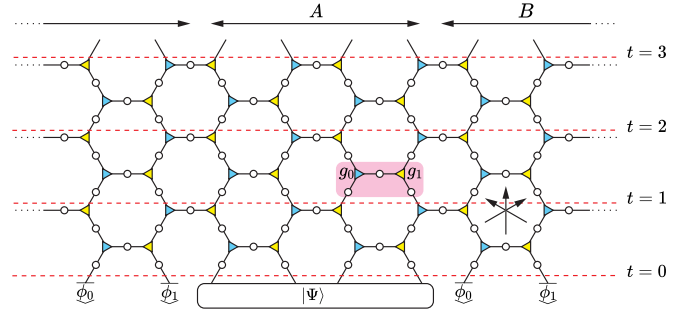


FIG. 1. Quantum circuit representation of the AKIM as a tensor network (unnormalized). The circuit is built up from two-local 2DU gates  $u(g_0, g_1)$  (pink shaded box) tiled in a brickwork pattern. The blue (yellow) triangles on the vertices carry phase factor  $g_0$  ( $g_1$ ). This representation makes evident that there are three ‘arrows of time’: ‘evolution’ of the circuit along any one of the black arrows appears unitary.

cently introduced by [31]. Similarly to the case of regular dual-unitarity (which may be termed the ‘first level’ (1DU) of an overarching bigger hierarchy), 2DU relates properties of the local quantum gates under a space-time rotation, but now of *pairs* of them, allowing for analytic tractability in the computation of spatiotemporal correlations.

Here, we show that because of these intriguing properties, the family of quantum circuits originating from “alternating kicked Ising models” has local entanglement dynamics that can be efficiently classically computed for all times. Moreover, under certain conditions, this can be analytically solved, displaying rich phenomenology. Interestingly, we find that dynamics ranges from quantum chaotic, to non-chaotic but which is neither Bethe-integrable nor Clifford. Our results extend our knowledge of solvable interacting quantum dynamics, yielding

yet more analytical testbeds to probe interesting physical phenomena like thermalization and beyond [32–35], quantum chaos [36, 37], novel dynamical phases in monitored quantum circuits [38–43], as well as the scrambling of quantum information [7, 8, 10].

*Model.*— We first focus on systems of qubits for ease of exposition, which has local Hilbert-space dimension  $q=2$ , leaving the discussion of the general case of qudits to later. We consider discrete-time dynamics under the “alternating kicked Ising model” (AKIM) acting on a 1D chain of qubits, with each time step  $t \in \mathbb{N}$  governed by the unitary  $U = U_e U_o$ , where  $U_{o/e} = e^{-iH^{(o/e)}} e^{ih \sum_{i=1} \sigma_i^y}$  and

$$H^{(o/e)} = J \sum_{\substack{(i,i+1) \in \\ \text{odd/even bonds}}} Z_i Z_{i+1} + \sum_i (g_i \bmod 2/2 + \pi/4) Z_i. \quad (1)$$

Here  $X_i, Y_i, Z_i$  are the standard Pauli matrices on site  $i$ . The unitary  $U$  describes time-evolution alternating between two Ising models which act only on odd or even bonds with strength  $J$ , subject to dimerized longitudinal fields  $g_0, g_1$ , and interrupted by global transverse kicks of strength  $h$ . We take  $J = h = \pi/4$ , and allow  $g_0, g_1$  to be arbitrary. Defined this way, the dynamics repeats periodically in time, i.e., is Floquet, but our analysis can be readily extended to allow for spatio-temporally random longitudinal fields. We note that due to reflection symmetry, dynamics at  $(g_0, g_1)$  is equivalent to that at  $(g_1, g_0)$ , and so we focus on the regime  $0 \leq g_0 \leq g_1 \leq 2\pi$ .

The physical setting of concern is of local thermalizing dynamics following a quantum quench. Concretely, we focus on a small contiguous subsystem  $A$  of even number of qubits  $N_A$  deep in the bulk and prepared in pure state  $|\Psi\rangle$ , as illustrated in Fig. 1; and assume the infinitely-large complement  $B$  is prepared as a dimerized product state  $\prod_i |\phi_0\rangle_{2i-1} |\phi_1\rangle_{2i}$ . We track  $A$ ’s state over time, given by the reduced density matrix (RDM)  $\rho_A(t)$ . In particular, we are interested in the dynamics of entanglement, quantified by the von Neuman entropy  $S(t) = -\text{Tr}(\rho_A(t) \log_2 \rho_A(t))$ , a proxy for the degree of quantum thermalization.

*Quantum circuit equivalent  $\mathcal{E}$  generalized dual-unitarity.*— We begin by observing that  $U^t$ , the time-evolution operator governing dynamics up to time  $t$ , can be equivalently written as a brickwork quantum circuit composed of the following two-local gates:

$$u(g_0, g_1) = (P(g_0) \otimes P(g_1)) CZ(H \otimes H), \quad (2)$$

where  $CZ, H, P(g_i) = \text{diag}(1, e^{ig_i})$  are the standard qubit control-Z, Hadamard, and phase gates of quantum computing respectively. Note that when  $g_0 = g_1 = 0$ ,  $u$  is equivalent (locally) to the CNOT gate, such that the circuit describes the kinetically-constrained deterministic Floquet quantum East model (DFQE) [44–47], whose entanglement dynamics was recently solved in [45]. While the techniques we employ bear similarities to that of

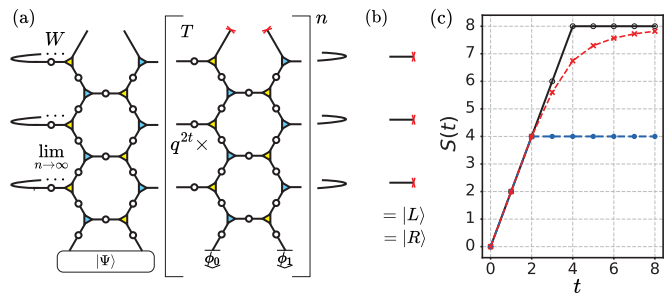


FIG. 2. (a) Computation of RDM  $\rho_A(t)$  using spatial transfer matrices  $T$  and temporal-to-spatial map  $W$ , as described in the main text. (b) Left and right eigenvectors of  $T$ : a product of  $t$  Bell states. (c) Entanglement dynamics of  $A$  with  $N_A=8$ . Black line: Dynamics of maximum-entanglement-solvable dimerized product states at  $g_0=0$  (arbitrary  $g_1$ ), as well as  $g_0=g_1=\pi/2$ , showcasing linear ramp with rate 2 till saturation at maximal entropy. Blue dash: Dynamics of  $|z\rangle|z\rangle \cdots$  at  $g_0=g_1=\pi/2$ , showing exact linear ramp till saturation at  $N_A/2$ . Red dash: Dynamics of  $|z\rangle|z\rangle \cdots$  at  $(g_0, g_1) = (5\pi/16, 7\pi/16)$ . Only at early times  $t \leq N_A/4$  is there an exact linear ramp; beyond which the approach to maximum entropy becomes exponential.

[45], what our work advances conceptually is the elucidation of how the DFQE lies in a much more general class of entanglement-solvable quantum circuits, generated by the AKIM.

To proceed, we introduce a tensor network (TN) representation: we first define basic tensors

$$\begin{array}{c} z_2 \\ | \\ g \\ | \\ z_1 \end{array} \begin{array}{c} z_3 \\ | \\ \delta_{z_1 z_2 z_3} e^{ig^{(z_1)}} \\ | \\ z_1 \end{array}, \quad \begin{array}{c} z_2 \\ | \\ \circ \\ | \\ z_1 \end{array} = (-1)^{z_1 z_2} / \sqrt{2}, \quad (3)$$

which describe a 3-legged Kronecker delta with phase  $g$  and Hadamard respectively (indices  $z_i \in \{0, 1\}$ ). Using standard rules of TN manipulations, we can build up the local gate  $u(g_0, g_1)$  as shown in Fig. 1, and hence the global circuit  $U^t$ , (see [47] for details). We find that  $U^t$  describes a tiling of space-time by a decorated hexagonal lattice. The diagrammatic representation makes immediately manifest that there are three “arrows of time”, due to similarity of the tensor network under  $120^\circ$  rotations: viewing the circuit (staying away from boundaries) as propagating a quantum state living on the line perpendicular to any one of the black arrows of Fig. 1, the corresponding evolution is unitary. This property can be termed ‘tri-unitarity’ [30], though we stress it is present at the global circuit level and not at the individual local gate level (further we do not find an obvious ‘blocking’ of local gates to form a tri-unitary gate). Instead, we observe the local gates possess a relation governing contractions of pairs of them along the space direction, termed

“second-level dual unitarity” (2DU) [31]:

$$(4)$$

Above, we have introduced bold tensors representing the folding of forward and backward branches of evolution, such as

$$(5)$$

which are the folded local gate  $u \otimes u^*$  and trace operation respectively. All these special properties hint at the analytical tractability of computing entanglement dynamics in these circuits, as we shall see.

*Exact influence matrices.*—We employ the powerful technique of space-time duality [48–52] to exchange the roles of space and time (i.e., rotate the TN by  $90^\circ$ ) and interpret dynamics as arising in the spatial direction. To illustrate the insight gained, we see the RDM  $\rho_A(t)$  can be computed by raising to a high power ‘spatial transfer matrices’  $T$ , inserting the operator  $W$  mapping temporal information to the spatial region  $A$ , before tracing over the temporal degrees of freedom, see Fig. 2(a). Now, due to unitarity and locality of the original dynamics, it can be shown that  $T$  has only a single eigenvalue 1, with all other eigenvalues 0 with Jordan blocks bounded in size by  $2t$ , so that  $T^{n \geq 2t} = |R\rangle\langle L|$ , where  $\langle L|, |R\rangle$  are the left and right eigenvectors respectively satisfying  $\langle L|T = \langle L|$  and  $T|R\rangle = |R\rangle$  [45, 50]. These eigenvectors are also called “influence matrices” (IM), as they effectively encode the effect of the bath on the subsystem as a quantum state living on the temporal direction [50, 53, 54]. The computation of  $\rho_A(t)$  in a thermodynamically large system thus simplifies to  $\langle L|W|R\rangle$ .

Generally, the form of an influence matrix in a strongly-interacting system is complicated and has no closed form expression [53, 55, 56]. However, for the AKIM, if we impose that the dimerized product state  $|\phi_0\rangle|\phi_1\rangle \cdots$  on  $B$  satisfies the *solvable IM conditions* (SIC):

$$(6)$$

which in equations read  $\langle R_x(g_0)^\dagger Z R_x(g_0) \rangle_0 \langle X \rangle_1 = 0$  and  $\langle X \rangle_0 \langle R_x(g_1)^\dagger Z R_x(g_1) \rangle = 0$  respectively, we find that  $|L\rangle = |R\rangle$  and admits the simple form of a product of  $t$  Bell pairs, see Fig. 2(b) and [47]. Above,  $R_x(g_i)$  denotes rotation about the  $x$ -axis by angle  $g_i$ . We see that the IM for the AKIM is identical to that of 1DU circuits (both within solvable states): it has zero temporal entanglement—that is, has trivial correlations in

time, and therefore describes the effect of the bath as a perfect Markovian dephaser on the boundaries. Proving this statement involves straightforward TN manipulations while using the tri-unitary (or 2DU) conditions, for example deriving  $T|R\rangle = |R\rangle$  for  $t = 2$  proceeds as follows:

$$(7)$$

where we used unitarity along the black arrows to remove the gates shaded in green, before we finally invoke SIC. Full details are in [47].

We thus establish our first result:  $\rho_A(t)$  can be exactly computed by repeatedly applying the quantum channel  $\mathcal{C}$  for  $t$  times:  $\rho_A(t) = \mathcal{C}^t [|\Psi\rangle_A \langle \Psi|_A]$ , where

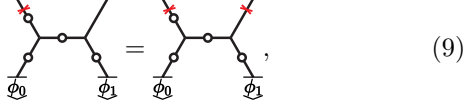
$$(8)$$

Note  $\mathcal{C}$  is unital:  $\mathcal{C}[I_A] = I_A$ , i.e., the infinite-temperature state  $\rho_{T=\infty} = I_A/2^{N_A}$  is a steady-state of dynamics, though there can be more. Physically,  $\mathcal{C}$  describes evolution under the AKIM on region  $A$  for one time-step, followed by dephasing on the boundaries. We emphasize that this result amounts to a tremendous reduction of the complexity of the problem, as it entails an efficient classical protocol to compute local dynamics even in a thermodynamically large, interacting system. Of course, the cost of computation does depend on the subsystem size  $N_A$ , but the point is that it is independent of the total system size  $N$ .

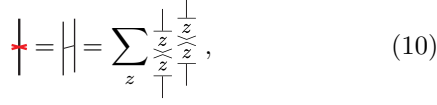
*Solvable entanglement dynamics*— Next, we consider the generation of entanglement entropy within region  $A$ . Most generally, for any  $(g_0, g_1)$ , we find that if states in  $A$  are also prepared in dimerized product states satisfying SIC, then we can prove  $S(t) = 2t$  for  $t \leq N_A/4$  (‘early-time regime’). Diagrammatically, this is done by evaluating the TN corresponding to the generalized purity  $\text{tr}(\rho_A^n(t))$  for all  $n \in \mathbb{N}$  and taking the limit  $\lim_{n \rightarrow 1} S_n(t)$  where  $S_n(t) = \frac{1}{1-n} \log \text{tr}(\rho_A^n(t))$  is the  $n$ -th Rényi entropy. Because of causality and short times, the TN factorizes into two disconnected terms, and tri-unitary/2DU allows us to fully contract the resulting circuit (see [47] for details).

When  $(g_0, g_1)$  are tuned to specific values, additional analytic structure arises allowing for efficient contraction of the TN even beyond early times. When  $g_0 = 0$  or  $\pi$  with arbitrary  $g_1$ , there exists a set of local TN identities enabling us to prove  $\mathcal{C}^{N_A+1} = \mathcal{C}^{N_A}$ , and that  $\rho_{T=\infty}$  is the only non-trivial eigenvector [47]. This implies that

any initial state  $|\Psi\rangle$  thermalizes *exactly* to the infinite-temperature state in at most finite time  $t = N_A$ . However, there are many states which equilibrate faster: if dimerized product states on  $A$  satisfy SIC and additionally *solvable entanglement conditions* (SEC):

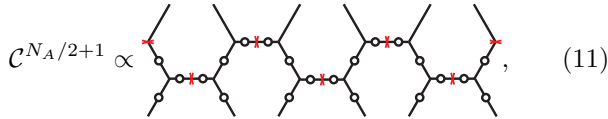


where the red cross in the middle of an edge



is defined as a projector pinning the forwards and backwards branches into the same computational basis state, then provably  $S(t) = \min(2t, N_A)$ , see Fig. 2(c). These “maximum-entanglement-solvable” states are exhausted by  $|\phi_0\rangle|\phi_1\rangle \in \{|z\rangle \otimes e^{i\theta X}|0\rangle\} \cup \{|\pm\rangle \otimes e^{i\theta' Z}|+\rangle\}$ , where  $X|\pm\rangle = \pm|\pm\rangle$ . We note the rate of entanglement generation is half the maximum possible in local brickwork circuits, achieved in 1DU circuits [57]. This is consistent with the results of a very recent work exploring speeds of quantum information propagation in 2DU circuits [58] (here, their  $n_A = d$ , predicting an asymptotic entanglement velocity  $v_E = 1/2$ ; however we stress our finding holds even non-asymptotically). Technically, the SEC allows to “transport” the red cross horizontally across the circuit, which physically amounts to spreading the effect of dephasing originally localized on the boundary into the bulk, resulting in a state that becomes mixed relatively more quickly. Of course, a computation within the TN representation is needed to make this observation quantitative [47].

When  $g_0 = g_1 = \pi/2$ , (or  $3\pi/2$ ), instead another set of local tensor network identities hold so that  $\mathcal{C}^{N_A/2+1} = \mathcal{C}^{N_A/2+2}$ . Physically, this implies that system equilibrates exactly at finite time  $t = N_A/2 + 1$  for a generic state [47]. However, interestingly,  $\rho_{T=\infty}$  is now not the only steady-state — the equilibrium state need not have maximal entropy. To understand what the additional steady-states are, we find that the TN of the late-time channel has the form



and read-off from it that  $\mathcal{C}^{N_A/2+1} = b_1 \circ b_{N_A} \circ \prod_{\text{even bonds}} c_{i,i+1} \circ \prod_{\text{odd bonds}} d_{i,i+1}$ , where  $b_i$  is the local  $Z$ -dephasing channel on site  $i$ , and  $c(d)_{i,i+1}$  are the  $ZZ(XX)$ -dissipative channels on sites  $i, i+1$ . For example,  $c_{i,i+1}[\rho] = \frac{1}{2}(\rho + Z_i Z_{i+1} \rho Z_i Z_{i+1})$ . It is straightforward to check there are  $2^{N_A-1}$  independent operators invariant under  $\mathcal{C}$ , given by all products of  $Z_i Z_{i+1}$

on odd bonds and  $X_i X_{i+1}$  on even bonds, for example  $ZYXII\dots$  and  $IXXII\dots$  i.e., this is a *super-extensive* set of conserved quantities. Focusing now on the family of dimerized initial states  $|\phi_0\rangle|\phi_1\rangle \in \{|z\rangle \otimes e^{i\theta Z}|+\rangle\} \cup \{|y, \pm\rangle \otimes e^{i\phi X}|0\rangle\}$  as well as those related by  $\phi_0 \leftrightarrow \phi_1$  (note these states satisfy SIC; here  $Y|y, \pm\rangle = \pm|y, \pm\rangle$ ), we can show that these states have zero expectation values within the conserved quantities and moreover have entanglement dynamics with an exact linear ramp, so that again  $S(t) = \min(2t, N_A)$ . We dub these “maximum-entanglement-solvable” states too. For  $|z\rangle|z\rangle\dots$  instead, our TN analysis yields  $S(t) = \min(2t, N_A/2)$ . These are illustrated in Fig. 2(c).

When  $(g_0, g_1) = (\pi/2, 3\pi/2)$ , the situation is richer as we find  $\mathcal{C}$  has now some eigenvectors with eigenvalues  $-1$ , indicating that the system generically does not equilibrate but rather oscillates at late times! This stems from the facts that (i) states satisfying SIC at parameters  $(g_0, g_1) = (\pi/2, \pi/2)$  are identical to those at  $(\pi/2, 3\pi/2)$ , and (ii) the action of the channel in the latter case (let us label it  $\mathcal{C}_{1/2,3/2}$ ) applied  $t$  times is equal to that of the former (let us label it  $\mathcal{C}_{1/2,1/2}$ ) applied  $t$  times, followed by the action of a Pauli channel which cycles between  $IYIY\dots, YYYY\dots, YIYI\dots, IIII\dots$  beginning at  $t = 1$ . This arises from the circuits’ Clifford nature [47]. For example, for  $t = (4n+1)$ ,  $n \in \mathbb{N}$ ,  $\mathcal{C}_{1/2,3/2}^t = \mathcal{P}_{IY} \circ \mathcal{C}_{1/2,1/2}^t$ , where  $\mathcal{P}_{IY}[\rho] := (IYIY\dots)\rho(IYIY\dots)$ . Now, since we know the invariant operators of  $\mathcal{C}_{1/2,1/2}^t$  at late times ( $t \geq N_A/2 + 1$ ), which we observe all commute with  $YYYY\dots$  but not all with  $IYIY\dots$  or  $YIYI\dots$ , it follows that  $\mathcal{C}_{1/2,3/2}^t = \mathcal{C}_{1/2,1/2}^t$  for late  $t$  which is even while  $\mathcal{C}_{1/2,3/2}^t = \mathcal{P}_{IY} \circ \mathcal{C}_{1/2,1/2}^t$  for late  $t$  which is odd. Therefore, unless the initial state has no overlap with the conserved quantities which are odd under  $IYIY\dots$ , the system will oscillate between two configurations indefinitely. However, we note that for considerations of the entanglement entropy, since the action of a Pauli channel is factorizable into tensor products of local channels, entanglement dynamics of the AKIM at  $(\pi/2, \pi/2)$  and  $(\pi/2, 3\pi/2)$  are identical for the same state.

Lastly, for generic  $(g_0, g_1)$  away from the aforementioned special parameter lines/points, we numerically find that  $\rho_{T=\infty}$  is the unique unity eigenvector of  $\mathcal{C}$ , while there are now eigenvectors with non-zero eigenvalues  $\lambda$ . The spectral gap  $\Delta := 1 - \max_{\lambda: |\lambda| < 1} |\lambda|$  determines the rate of thermalization (see [47] for a numerical analysis). We also do not find any obvious simple product states whose entanglement dynamics can be analytically understood beyond the early-time regime, which as discussed are exhibited by SIC-satisfying states (Fig. 2(c)).

*Qudit generalization.*—The AKIM and resulting circuit with generalized dual-unitarity can be straightforwardly extended to chains of qudits of arbitrary local Hilbert-space dimension  $q$ , and similar statements of solvable entanglement dynamics derived. The

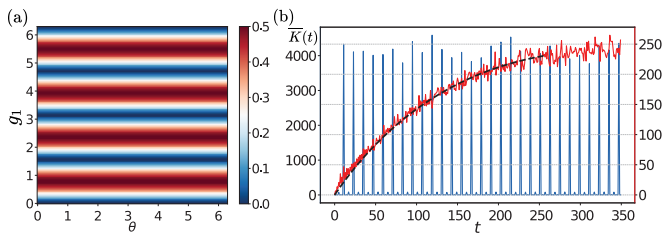


FIG. 3. (a) Operator entanglement of a stabilizer at intermediate times underpinning the RDM  $\rho_A(t)$ , as a function of phase  $g_1$  and angle  $\theta$  parameterizing the initial state. The stabilizer generally has non-trivial operator entanglement entropy, indicating complex structure in space that cannot be exhibited by Pauli stabilizers. (b) SFF of the AKIM at  $N_A = 8$ . Blue (left y-axis): SFF for  $g_0 = 0$ , shows regular revivals, different from Poissonian statistics (which would entail a constant SFF). Red (right y-axis): SFF for generic parameters falls within the COE class: the fit is to the RMT prediction  $2t - t \ln(1 + 2t/2^{N_A})$  [59]. Note the differences in scale.

key is to observe that all diagrammatic relations of the basic tensors, which underlie the contractibility of the TN and hence solvability of the dynamics, are preserved upon generalization of the phase gate  $P(g) \mapsto P(\vec{g}) = \text{diag}(1, e^{ig^{(1)}}, \dots, e^{ig^{(q-1)}})$ , and the Hadamard transform to the  $q$ -dimensional quantum Fourier transform operator  $H$  ( $H_{z_1 z_2} = \omega^{z_1 z_2} / \sqrt{q}$ , where  $0 \leq z_i \leq q - 1$  and  $\omega = e^{i2\pi/q}$ ). A thorough discussion is given in [47].

*Discussion.*—We have introduced the AKIM, and demonstrated how its entanglement dynamics can be efficiently and at times fully solved, enabled by properties of generalized dual-unitarity. It is interesting to contrast our findings to other known analytically-solvable models of quantum dynamics. To the best of our knowledge, our model is not integrable nor dual-unitary. More interesting though, is the connection to Clifford dynamics—dynamics under gates which preserve the Pauli group [20–23]. On one hand, our calculation of the generalized purities in the entanglement solvable cases also yields that the entanglement spectrum of  $\rho_A(t)$  (negative logarithm of its eigenvalues) is flat [47], a feature exhibited too by Clifford dynamics [21]. On the other hand, only parameters  $(g_0, g_1) = (n\pi/2, m\pi/2)$  of the AKIM where  $n, m \in \mathbb{Z}$ , constitute Clifford circuits, while we have shown that full entanglement-solvability extends beyond these isolated points. Moreover, even when the AKIM is Clifford, the entanglement-solvable states need not be Pauli-stabilized states, a condition otherwise needed in order for the Gottesman-Knill theorem of efficient classical simulability to apply [20, 60].

To drive home the difference with Clifford evolution, we investigate the decomposition of the RDM  $\rho_A(t)$  at various times, for parameters  $g_0 = 0$  and arbitrary  $g_1$ , as well as dimerized initial states  $|0\rangle \otimes e^{i\theta X}|0\rangle$  on  $A$ , into the product of orthogonal projectors onto eigenspaces

defined by stabilizers  $\rho_A(t) \propto \prod_i (1 + O_i)$ . Here the stabilizers  $O_i$  are defined to be mutually commuting, each having equal numbers of  $\pm 1$  eigenvalues, but need not be a Pauli string. We show in Fig. 3(a) a characterization of the spatial structure of a representative  $O_i$  at a later time: we see it generically develops operator entanglement—entropy related to non-factorizability into a tensor product of locally-supported operators for some bipartition of space (details of the calculation are in [47]). In contrast, Pauli stabilizers undergoing Clifford evolution can never develop operator entanglement [20, 61]. Moreover, a quick computation of the spectral form factor (SFF)  $\bar{K}(t) = |\text{tr}(U^t)|^2$  [24, 62] for  $g_0 = 0$  (averaging over spatially-random  $g_1$  uniformly), yields spectral statistics that appears neither Poissonian, Wigner-Dyson, nor consistent with those of Clifford circuits (see e.g. [22]). In contrast, uniformly averaging over  $g_0, g_1$  yields spectral statistics agreeing perfectly with the circular orthogonal ensemble (COE) of random matrix theory (RMT) [59]. All these indicate that the physics of the AKIM is very rich, capturing both quantum chaos, as well as an interesting conceptually novel class of non-chaotic but still analytically-solvable quantum dynamics, which deserves to be better characterized.

*Acknowledgments.* We thank Katja Klobas, Bruno Bertini and Huang Qi for interesting discussions. W. W. H. is supported by the Singapore NRF Fellowship, NRF-NRFF15-2023-0008, and the CQT Bridging Fund.

\* c.liu@u.nus.edu

† wenweiho@nus.edu.sg

- [1] M. Rigol, V. Dunjko, and M. Olshanii, *Nature* **452**, 854 (2008).
- [2] R. Nandkishore and D. A. Huse, *Annual Review of Condensed Matter Physics* **6**, 15–38 (2015).
- [3] L. D’Alessio, Y. Kafri, A. Polkovnikov, and M. Rigol, *Advances in Physics* **65** (2016), 10.1080/00018732.2016.1198134.
- [4] D. A. Abanin, E. Altman, I. Bloch, and M. Serbyn, *Rev. Mod. Phys.* **91**, 021001 (2019).
- [5] P. Hayden and J. Preskill, *Journal of High Energy Physics* **2007**, 120–120 (2007).
- [6] S. H. Shenker and D. Stanford, *Journal of High Energy Physics* **2014**, 67 (2014).
- [7] P. Hosur, X.-L. Qi, D. A. Roberts, and B. Yoshida, *J. High Energ. Phys.* **2**, 4 (2016).
- [8] D. A. Roberts and B. Yoshida, *Journal of High Energy Physics* **2017**, 121 (2017).
- [9] M. Mezei and D. Stanford, *Journal of High Energy Physics* **2017**, 65 (2017).
- [10] K. A. Landsman, C. Figgatt, T. Schuster, N. M. Linke, B. Yoshida, N. Y. Yao, and C. Monroe, *Nature* **567**, 61 (2019).
- [11] H. Aoki, N. Tsuji, M. Eckstein, M. Kollar, T. Oka, and P. Werner, *Rev. Mod. Phys.* **86**, 779 (2014).

- [12] G. Vidal, Phys. Rev. Lett. **91**, 147902 (2003).
- [13] A. J. Daley, C. Kollath, U. Schollwöck, and G. Vidal, Journal of Statistical Mechanics: Theory and Experiment **2004**, P04005 (2004).
- [14] S. Paeckel, T. Köhler, A. Swoboda, S. R. Manmana, U. Schollwöck, and C. Hubig, Annals of Physics **411**, 167998 (2019).
- [15] K. Hémerly, F. Pollmann, and D. J. Luitz, Phys. Rev. B **100**, 104303 (2019).
- [16] V. Alba and P. Calabrese, Proceedings of the National Academy of Sciences **114**, 7947 (2017).
- [17] F. H. L. Essler and M. Fagotti, Journal of Statistical Mechanics: Theory and Experiment **2016**, 064002 (2016).
- [18] P. Calabrese, SciPost Physics Lecture Notes, **20** (2020).
- [19] K. Klobas, B. Bertini, and L. Piroli, Phys. Rev. Lett. **126**, 160602 (2021).
- [20] M. A. Nielsen and I. L. Chuang, *Quantum Computation and Quantum Information* (Cambridge University Press, Cambridge, 2000).
- [21] A. Nahum, J. Ruhman, S. Vijay, and J. Haah, Phys. Rev. X **7**, 031016 (2017).
- [22] T. Farshi, J. Richter, D. Toniolo, A. Pal, and L. Masanes, PRX Quantum **4**, 030302 (2023).
- [23] J. Richter, O. Lunt, and A. Pal, Phys. Rev. Res. **5**, L012031 (2023).
- [24] B. Bertini, P. Kos, and T. Prosen, Phys. Rev. Lett. **121**, 264101 (2018).
- [25] S. Gopalakrishnan and A. Lamacraft, Phys. Rev. B **100**, 064309 (2019).
- [26] S. A. Rather, S. Aravinda, and A. Lakshminarayan, Phys. Rev. Lett. **125**, 070501 (2020).
- [27] L. Piroli, B. Bertini, J. I. Cirac, and T. c. v. Prosen, Phys. Rev. B **101**, 094304 (2020).
- [28] P. W. Claeys and A. Lamacraft, Phys. Rev. Lett. **126**, 100603 (2021).
- [29] A. Flack, B. Bertini, and T. Prosen, Phys. Rev. Res. **2**, 043403 (2020).
- [30] C. Jonay, V. Khemani, and M. Ippoliti, Phys. Rev. Res. **3**, 043046 (2021).
- [31] X.-H. Yu, Z. Wang, and P. Kos, “Hierarchical generalization of dual unitarity,” (2023), arXiv:2307.03138 [quant-ph].
- [32] W. W. Ho and S. Choi, Phys. Rev. Lett. **128**, 060601 (2022).
- [33] J. S. Cotler, D. K. Mark, H.-Y. Huang, F. Hernández, J. Choi, A. L. Shaw, M. Endres, and S. Choi, PRX Quantum **4**, 010311 (2023).
- [34] M. Ippoliti and W. W. Ho, Quantum **6**, 886 (2022).
- [35] M. Ippoliti and W. W. Ho, PRX Quantum **4**, 030322 (2023).
- [36] M. Srednicki, Physical Review E **50**, 888 (1994).
- [37] A. Chan, A. De Luca, and J. T. Chalker, Phys. Rev. X **8**, 041019 (2018).
- [38] B. Skinner, J. Ruhman, and A. Nahum, Phys. Rev. X **9**, 031009 (2019).
- [39] Y. Li, X. Chen, and M. P. A. Fisher, Phys. Rev. B **100**, 134306 (2019).
- [40] S. Choi, Y. Bao, X.-L. Qi, and E. Altman, Phys. Rev. Lett. **125**, 030505 (2020).
- [41] Y. Bao, S. Choi, and E. Altman, Phys. Rev. B **101**, 104301 (2020).
- [42] M. J. Gullans and D. A. Huse, Phys. Rev. Lett. **125**, 070606 (2020).
- [43] P. W. Claeys, M. Henry, J. Vicary, and A. Lamacraft, Phys. Rev. Res. **4**, 043212 (2022).
- [44] B. Bertini, P. Kos, and T. Prosen, arXiv:2306.12467 (2022).
- [45] B. Bertini, C. D. Fazio, J. P. Garrahan, and K. Klobas, “Exact quench dynamics of the floquet quantum east model at the deterministic point,” (2023), arXiv:2310.06128 [cond-mat.stat-mech].
- [46] N. Pancotti, G. Giudice, J. I. Cirac, J. P. Garrahan, and M. C. Bañuls, Phys. Rev. X **10**, 021051 (2020).
- [47] See Supplemental material online for details of tensor network notation and manipulation, as well as proofs of statements presented in the main text.
- [48] M. C. Bañuls, M. B. Hastings, F. Verstraete, and J. I. Cirac, Phys. Rev. Lett. **102**, 240603 (2009).
- [49] M. B. Hastings and R. Mahajan, Phys. Rev. A **91**, 032306 (2015).
- [50] A. Leroose, M. Sonner, and D. A. Abanin, Phys. Rev. X **11**, 021040 (2021).
- [51] T.-C. Lu and T. Grover, PRX Quantum **2**, 040319 (2021).
- [52] M. Ippoliti, T. Rakovszky, and V. Khemani, Phys. Rev. X **12**, 011045 (2022).
- [53] M. Sonner, A. Leroose, and D. A. Abanin, Annals of Physics **435**, 168677 (2021), special issue on Philip W. Anderson.
- [54] G. Giudice, G. Giudici, M. Sonner, J. Thoenniss, A. Leroose, D. A. Abanin, and L. Piroli, Phys. Rev. Lett. **128**, 220401 (2022).
- [55] A. Leroose, M. Sonner, and D. A. Abanin, Phys. Rev. B **104**, 035137 (2021).
- [56] A. Foligno, T. Zhou, and B. Bertini, Phys. Rev. X **13**, 041008 (2023).
- [57] T. Zhou and A. W. Harrow, Phys. Rev. B **106**, L201104 (2022).
- [58] A. Foligno, P. Kos, and B. Bertini, arXiv:2312.02940 [cond-mat, physics:quant-ph] (2023).
- [59] M. L. Mehta, *Random Matrices and the Statistical Theory of Spectra*, 2nd ed. (Academic, New York, 1991).
- [60] D. Gottesman, arXiv:quant-ph/9807006 (1998).
- [61] D. Fattal, T. S. Cubitt, Y. Yamamoto, S. Bravyi, and I. L. Chuang, (2004), arXiv:quant-ph/0406168 [quant-ph].
- [62] J. Liu, Phys. Rev. D **98**, 086026 (2018).

# Supplemental Information: Solvable entanglement dynamics in quantum circuits with generalized dual unitarity

Chuan Liu<sup>1,\*</sup> and Wen Wei Ho<sup>1,2,†</sup>

<sup>1</sup>*Department of Physics, National University of Singapore, Singapore 117542*

<sup>2</sup>*Centre for Quantum Technologies, National University of Singapore, 3 Science Drive 2, Singapore 117543*

(Dated: December 19, 2023)

In this supplemental information, we provide details on the tensor network (TN) analysis of the alternating kicked Ising model (AKIM) for systems of qudits with arbitrary local Hilbert space dimension, proofs of various statements on entanglement dynamics, as well as numerical investigations into the properties of the channel  $\mathcal{C}$  governing local dynamics and the fine-structure of stabilizers under entanglement-solvable dynamics.

Concretely, Sec. **I** describes the connection of the AKIM to the deterministic Floquet quantum East Model (DFQE). Sec. **II** presents the tensor network framework in which the analysis of the AKIM is performed in. Sec. **III** derives the fixed points of the spatial transfer matrix considered in the main text, i.e., the influence matrices (IM), as well as the structure of initial states satisfying the solvable influence-matrix conditions (SIC). Sec. **IV** derives the general result of exact early-time ( $t \leq N_A/4$ ) entanglement dynamics for dimerized initial states satisfying the SIC. Sec. **V** focuses on entanglement dynamics of the AKIM with  $\vec{g}_0 = \vec{0}$  and arbitrary  $\vec{g}_1$ , in particular on the maximum-entanglement-solvable states. Sec. **VI** describes the entanglement dynamics of the AKIM on qubits at parameter regimes harboring degenerate steady-states (this is given by  $g_0 = (2n+1)\pi/2$ ,  $g_1 = (2m+1)\pi/2$ , with  $n, m \in \mathbb{Z}$ ). Sec. **VII** explores numerically the gap of the channel  $\mathcal{C}$  governing thermalizing dynamics of a local region, which sets the rate of thermalization. Sec. **VIII** investigates the spatial structure of stabilizers underlying the reduced density matrix arising in dynamics from maximum-entanglement-solvable states, in particular probing their operator entanglement entropy.

## I. RELATION TO THE DETERMINISTIC FLOQUET QUANTUM EAST MODEL

Here, we illustrate the connection of the AKIM (on qubits) to the deterministic Floquet quantum East model [1, 2] (DFQE), whose entanglement dynamics was recently solved by [2]. It is an example of a kinetically constrained model, and is given as a brickwork circuit with two-local gates acting on a chain of qubits:

$$w = \mathbb{I} \otimes \bar{P} + X \otimes P, \quad (1)$$

where the projector  $P = \mathbb{I} - \bar{P} = (\mathbb{I} + Z)/2$ . The action of the gate is as such: when the control (right qubit) is in state  $|0\rangle$ , the target (left qubit) is left unchanged; while if the control is in  $|1\rangle$ , the target is flipped ( $|z\rangle \rightarrow X|z\rangle$ , where  $z = 0, 1$ ). In other words,  $w$  is a CNOT gate.

The two-local gates we introduced in the main text,

$$u(g_0, g_1) = (P(g_0) \otimes P(g_1))CZ(H \otimes H), \quad (2)$$

are related to  $w$  via

$$w = (H \otimes I)u(0, 0)(\mathbb{I} \otimes H). \quad (3)$$

Thus, the two global circuits (AKIM and DFQE) are unitarily related by a tensor product of local unitaries:

$$U_{\text{DFQE}}^t = (\cdots \mathbb{I} \otimes H \otimes \mathbb{I} \otimes H \cdots) U_{\text{AKIM}}^t(g_0 = g_1 = 0) (\cdots \mathbb{I} \otimes H \otimes \mathbb{I} \otimes H \cdots), \quad (4)$$

implying that the entanglement dynamics of state  $|\Psi\rangle$  under the DFQE and  $(\cdots \mathbb{I} \otimes H \otimes \mathbb{I} \otimes H \cdots)|\Psi\rangle$  under the AKIM (at  $g_0 = g_1 = 0$ ) are identical.

---

\* c'liu@u.nus.edu

† wenweiho@nus.edu.sg

## II. TENSOR NETWORK REPRESENTATION OF AKIM

### A. Basic TN diagrams

In this section, we introduce the general tensor network notation used to analyze the circuit generated by the AKIM in arbitrary local qudit dimensions  $q$  (the main text focused on the qubit case). We note the AKIM can be always written as a Hamiltonian using clock and shift operators acting on a  $q$ -dimensional local space (defined below), which are the generalization of Pauli qubit operators, but we leave the explicit form as an exercise to the reader. The two basic tensors which form the building blocks of the quantum circuit are:

$$\begin{array}{c} z_2 \\ \diagdown \\ \vec{g} \\ \diagup \\ z_1 \end{array} \text{---} z_3 = \delta_{z_1 z_2 z_3} e^{ig^{(z_1)}}, \quad \begin{array}{c} z_2 \\ | \\ \circ \\ | \\ z_1 \end{array} := H_{z_1 z_2} = \frac{1}{\sqrt{q}} \omega^{z_1 z_2}. \quad (5)$$

The first tensor has three legs and is labeled by a  $q$ -dimensional vector  $\vec{g} = (1, g^{(1)}, g^{(2)}, \dots, g^{(q-1)})$ , and denotes a generalized Kronecker-delta function  $\delta_{z_1 z_2 z_3} e^{ig^{(z_1)}}$  which enforces all inputs to be equal in the computational basis  $z = 0, 1, \dots, q-1$ , upon which it evaluates to the phase  $e^{ig^{(z_1)}}$ , otherwise it vanishes. The second tensor is the quantum Fourier transform operator, with matrix elements in the computational basis given by the discrete Fourier transform matrix  $H_{z_1 z_2} = \frac{1}{\sqrt{q}} \omega^{z_1 z_2}$  where  $\omega = e^{i2\pi/q}$ . When  $q = 2$  (qubit), this reduces to the familiar Hadamard matrix  $H = \frac{1}{\sqrt{2}} \begin{pmatrix} 1 & 1 \\ 1 & -1 \end{pmatrix}$ .

We will also find it useful to introduce tensors denoting the  $q$ -dimensional clock and shift operators respectively,

$$\begin{array}{c} z_2 \\ | \\ \boxed{Z}^j \\ | \\ z_1 \end{array} := Z_{z_1 z_2}^j = \delta_{z_1 z_2} \omega^{z_1 j}, \quad \begin{array}{c} z_2 \\ | \\ \boxed{X}^j \uparrow \\ | \\ z_1 \end{array} := X_{z_1 z_2}^j = \begin{cases} 0, & z_2 \equiv z_1 + j \pmod{q} \\ 1, & z_2 \not\equiv z_1 + j \pmod{q} \end{cases} \quad (6)$$

Above,  $j$  denotes the integer power that the operator is raised to, and is not an index. Note that because the shift operator  $X$  is not symmetric in general (i.e.,  $X^T \neq X$ ), we have also drawn an arrow in the diagram for  $X$  to denote the direction of its right action. For quantum states, their TN representation is simply

$$\frac{1}{\sqrt{q}} := |\phi_1\rangle. \quad (7)$$

Following standard TN rules on contracting tensors (one can join tensors by connecting legs and summing over the underlying indices), we can produce derivative tensors. For example, we can compute the following diagram

$$u(\vec{g}_0, \vec{g}_1) = \sqrt{q} \begin{array}{c} \diagdown \quad \diagup \\ \vec{g}_0 \quad \vec{g}_1 \\ \diagup \quad \diagdown \\ \circ \quad \circ \end{array} = (P(\vec{g}_0) \otimes P(\vec{g}_1)) CZ(H \otimes H), \quad (8)$$


which describes the two-local qudit gate  $u(\vec{g}_0, \vec{g}_1)$  that builds up the brickwork circuit of the AKIM. Here,  $CZ := \text{diag}(\underbrace{1, 1, \dots, 1}_q, \underbrace{1, \omega, \dots, \omega^{q-1}}_q, \dots, \underbrace{1, \omega^{q-1}, \dots, \omega^{q(q-1)}}_q)$  and  $P(\vec{g}_i) := \text{diag}(1, e^{ig_i^{(1)}}, e^{ig_i^{(2)}}, \dots, e^{ig_i^{(q-1)}})$  are the generalized control-Z and phase gates respectively, for qudits. In the qubit case, this reduces to the familiar  $CZ = \text{diag}(1, 1, 1, -1)$  and  $P(g_i) = \text{diag}(1, e^{ig_i})$ .

### B. TN in folded representation

In the study of quantum dynamics, we routinely consider objects like  $|\Psi(t)\rangle = U(t)|\Psi(0)\rangle \langle\Psi(0)|U(t)^\dagger$  and  $\rho_A(t) = \text{tr}_B |\Psi(t)\rangle \langle\Psi(t)|$ . We see that this always involves the forwards and backwards branches of time-evolution together (and more pairs of forwards and backwards branches if we are computing, say, the entanglement entropy). It is convenient to vectorize the adjoint map  $U[\cdot]U^\dagger$  into a matrix acting on a doubled Hilbert space  $U \otimes U^*$ , which



amounts to ‘folding’  $U^\dagger$  into  $U^*$ , as well as vectorize the quantum state  $|\phi\rangle\langle\phi| \mapsto |\phi\rangle \otimes |\phi\rangle^*$ . To represent these in TN notation, we introduce bold tensors, for example of the local gates and local states  $u \otimes u^*$  and  $|\phi_1\rangle \otimes |\phi_1\rangle^*$



$$\text{Diagrammatic equation (9)} \quad (9)$$

Then the trace operation (on one qubit) and the projector  $\sum_z |zz\rangle\langle zz|$  pinning forwards and backwards branches (which will routinely show up) can be diagrammatically represented as



$$\text{Diagrammatic equation (10)} \quad (10)$$

Using these bold folded tensors, we can carry out diagrammatic calculations very compactly. For example the unitarity of the gates Eq. (8) can be expressed



$$\text{Diagrammatic equation (11)} \quad (11)$$

which represents  $u^\dagger u = \mathbb{I}$  (in unfolded language), while



$$\text{Diagrammatic equation (12)} \quad (12)$$

represents  $uu^\dagger = \mathbb{I}$ . Another example is the overlap of states (assumed normalized)



$$\text{Diagrammatic equation (13)} \quad (13)$$

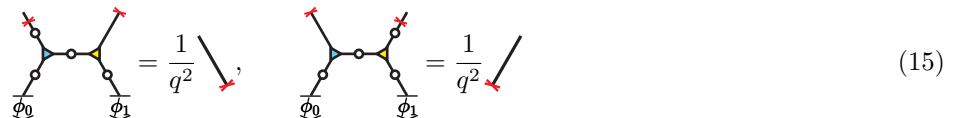
and the following will be extremely useful relations that we will routinely employ:



$$\text{Diagrammatic equation (14)} \quad (14)$$

### III. TRANSFER MATRIX AND INFLUENCE MATRICES

Here we provide additional details on the assertion in the main text that the influence matrices (both left and right) are a product of  $t$  Bell states, assuming that the system on  $B$  is prepared in a dimerized product state  $\prod_i |\phi_0\rangle_{2i-1} |\phi_1\rangle_{2i}$  which satisfies the *Solvable Influence-matrix Conditions* (SIC):



$$\text{Diagrammatic equation (15)} \quad (15)$$

Now, the right and left influence matrices  $|R\rangle$  and  $\langle L|$  are defined to be the unique (unique due to unitarity of the

original circuit) right and left eigenvector of  $T$  with unit eigenvalue [3], i.e.,  $T|R\rangle = |R\rangle$  and  $\langle L|T = \langle L|$ , where

$$T = q^{2t} \quad (16)$$

Note that it can also be shown all other eigenvalues of  $T$  are zero and its largest Jordan block is of size  $2t$  because of locality of the dynamics (see [2, 3]). Our claim is that for the AKIM with states satisfying SIC on  $B$ ,

$$|R\rangle = \begin{matrix} \text{---} \times \\ \text{---} \times \\ \text{---} \times \\ \text{---} \times \end{matrix}, \quad \langle L| = \begin{matrix} \times \text{---} \\ \times \text{---} \\ \times \text{---} \\ \times \text{---} \end{matrix}. \quad (17)$$

Notice that  $\langle L| = |R\rangle$ .

This can be proven straightforwardly, diagrammatically. We compute:

$$T|R\rangle = q^{2t} = q^{2t} = q^{t+1} = q^2 \begin{matrix} \text{---} \times \\ \text{---} \times \\ \text{---} \times \\ \text{---} \times \end{matrix} = \begin{matrix} \text{---} \times \\ \text{---} \times \\ \text{---} \times \\ \text{---} \times \end{matrix}, \quad (18)$$

where in the third and fourth equality, we continually use the triunitary/generalized dual-unitary property in the time direction represented by the arrows, to remove green shaded boxes (since it is unitary in that direction), while in the

last equality, we utilized SIC. Similarly, using generalized dual-unitarity and SIC we can compute

$$\langle L|T = q^{2t} = q^{2t} = q^{t+1} = q^2 \quad (19)$$

Given these influence matrices, the reduced density matrix for subsystem  $A$  deep inside the bulk then takes a simple form:

$$\rho_A(t) = q^{t(N_A - 1)} \quad (20)$$

and we see that it can be obtained by iterating the following quantum channel  $\mathcal{C}$ :

$$\mathcal{C} = q^{N_A - 1} \quad (21)$$

on the initial state  $|\Psi\rangle\langle\Psi|$ . This quantum channel is a composition of a unitary channel describing time-evolution by the AKIM in region  $A$ , as well as a channel describing  $z$ -dephasing on the boundaries.

### A. Solving the SICs

We show here that there are non-trivial solutions to the SICs. Explicitly, the SICs imply:

$$\begin{aligned}
\delta_{ij} = \begin{array}{|c} |j\rangle^\dagger \\ \hline |i\rangle \end{array} &= q^2 \begin{array}{|c} \widehat{\phi}_0^\dagger \quad \widehat{\phi}_1^\dagger \\ \hline \begin{array}{|c} |j\rangle^\dagger \\ \hline |i\rangle \end{array} \\ \hline \phi_0 \quad \phi_1 \end{array} = q \begin{array}{|c} \widehat{\phi}_0^\dagger \quad \widehat{\phi}_1^\dagger \\ \hline \begin{array}{|c} |i-j\rangle \\ \hline \end{array} \\ \hline \phi_0 \quad \phi_1 \end{array} \\
&= q \begin{array}{|c} \widehat{\phi}_0^\dagger \quad \widehat{\phi}_1^\dagger \\ \hline \begin{array}{|c} |i-j\rangle \\ \hline \end{array} \\ \hline \phi_0 \quad \phi_1 \end{array} = q \begin{array}{|c} \widehat{\phi}_0^\dagger \quad \widehat{\phi}_1^\dagger \\ \hline \begin{array}{|c} |i-j\rangle \\ \hline \end{array} \\ \hline \phi_0 \quad \phi_1 \end{array} = q \begin{array}{|c} \widehat{\phi}_0^\dagger \quad \widehat{\phi}_1^\dagger \\ \hline \begin{array}{|c} |i-j\rangle \\ \hline \end{array} \\ \hline \phi_0 \quad \phi_1 \end{array} = q \begin{array}{|c} \widehat{\phi}_0^\dagger \quad \widehat{\phi}_1^\dagger \\ \hline \begin{array}{|c} |i-j\rangle \\ \hline \end{array} \\ \hline \phi_0 \quad \phi_1 \end{array} \\
\end{aligned} \tag{22}$$

$$\begin{aligned}
\delta_{ij} = \begin{array}{|c} |j\rangle^\dagger \\ \hline |i\rangle \end{array} &= q^2 \begin{array}{|c} \widehat{\phi}_0^\dagger \quad \widehat{\phi}_1^\dagger \\ \hline \begin{array}{|c} |j\rangle^\dagger \\ \hline |i\rangle \end{array} \\ \hline \phi_0 \quad \phi_1 \end{array} = q \begin{array}{|c} \widehat{\phi}_0^\dagger \quad \widehat{\phi}_1^\dagger \\ \hline \begin{array}{|c} |i-j\rangle \\ \hline \end{array} \\ \hline \phi_0 \quad \phi_1 \end{array} \\
&= q \begin{array}{|c} \widehat{\phi}_0^\dagger \quad \widehat{\phi}_1^\dagger \\ \hline \begin{array}{|c} |i-j\rangle \\ \hline \end{array} \\ \hline \phi_0 \quad \phi_1 \end{array} = q \begin{array}{|c} \widehat{\phi}_0^\dagger \quad \widehat{\phi}_1^\dagger \\ \hline \begin{array}{|c} |i-j\rangle \\ \hline \end{array} \\ \hline \phi_0 \quad \phi_1 \end{array} = q \begin{array}{|c} \widehat{\phi}_0^\dagger \quad \widehat{\phi}_1^\dagger \\ \hline \begin{array}{|c} |i-j\rangle \\ \hline \end{array} \\ \hline \phi_0 \quad \phi_1 \end{array} = q \begin{array}{|c} \widehat{\phi}_0^\dagger \quad \widehat{\phi}_1^\dagger \\ \hline \begin{array}{|c} |i-j\rangle \\ \hline \end{array} \\ \hline \phi_0 \quad \phi_1 \end{array} \\
\end{aligned} \tag{23}$$

where we have defined the state  $|\hat{i}\rangle := H|i\rangle$ , and  $|i\rangle$  is the  $i$ th computational basis state. In Eq. (22) and Eq. (23), we have utilized the fact that

$$q \begin{array}{|c} \hline \circ^\dagger \\ \hline \begin{array}{|c} | \\ \hline \end{array} \\ \hline \begin{array}{|c} | \\ \hline \end{array} \\ \hline \end{array} = \begin{array}{|c} | \\ \hline \end{array} \begin{array}{|c} | \\ \hline \end{array}, \quad HZH^\dagger = X \tag{24}$$

Thus we can write down the SICs as two explicit equations:

$$\begin{aligned}
\langle R_x^\dagger(\vec{g}_0) Z^{-k} R_x(\vec{g}_0) \rangle_0 \langle X^k \rangle_1 &= 0, \\
\langle X^k \rangle_0 \langle R_x^\dagger(\vec{g}_1) Z^k R_x(\vec{g}_1) \rangle_1 &= 0
\end{aligned} \tag{25}$$

where  $R_x(\vec{g}) := H^\dagger P(\vec{g})H$  and  $k = 1, 2, \dots, q - 1$ . For qubits, Eq. (25) will reduced to:

$$\begin{aligned} \langle R_x(g_0)^\dagger Z R_x(g_0) \rangle_0 \langle X \rangle_1 &= 0, \\ \langle X \rangle_0 \langle R_x(g_1)^\dagger Z R_x(g_1) \rangle_1 &= 0. \end{aligned} \quad (26)$$

That is, the product of the expectation value of  $Z$  rotated around the  $x$ -axis by  $g_0$  and the expectation value of  $X$  is vanishing; and the product of the expectation value of  $X$  and the expectation value of  $Z$  rotated around the  $x$ -axis by  $g_1$  is vanishing, respectively. There is a large family of product states that satisfy these. For example, when  $g_0 = g_1 = 0$  (again for qubits), then the SICs reduce to

$$\begin{aligned} \langle Z \rangle_0 \langle X \rangle_1 &= 0, \\ \langle X \rangle_0 \langle Z \rangle_1 &= 0. \end{aligned} \quad (27)$$

The exhaustive set of solutions is the union of the sets  $\{e^{-i\theta Z}|+\rangle \otimes e^{-i\theta' Z}|+\rangle\}$ ,  $\{e^{-i\theta'' X}|0\rangle \otimes e^{-i\theta''' X}|0\rangle\}$ ,  $\{|y, \pm\rangle \otimes |\psi\rangle\}$ ,  $\{|\psi'\rangle \otimes |y, \pm\rangle\}$  where  $\theta, \theta', \theta'', \theta'''$  are arbitrary angles and  $|\psi\rangle, |\psi'\rangle$  are arbitrary qubit states. Here  $|+\rangle = \frac{1}{\sqrt{2}}(|0\rangle + |1\rangle)$  and  $|y, \pm\rangle = \frac{1}{\sqrt{2}}(|0\rangle \pm i|1\rangle)$ .

#### IV. EARLY TIME ENTANGLEMENT DYNAMICS OF SIC STATES: EXACT LINEAR RAMP

We first present general analytic statements that can be made for early time entanglement dynamics. In particular, we claim that if the initial state of the subsystem  $A$  is prepared in a dimerized product state that satisfies the SIC, then  $S(t) = 2t$  for  $0 \leq t \leq N_A/4$  (we remind the reader  $t \in \mathbb{N}$ ).

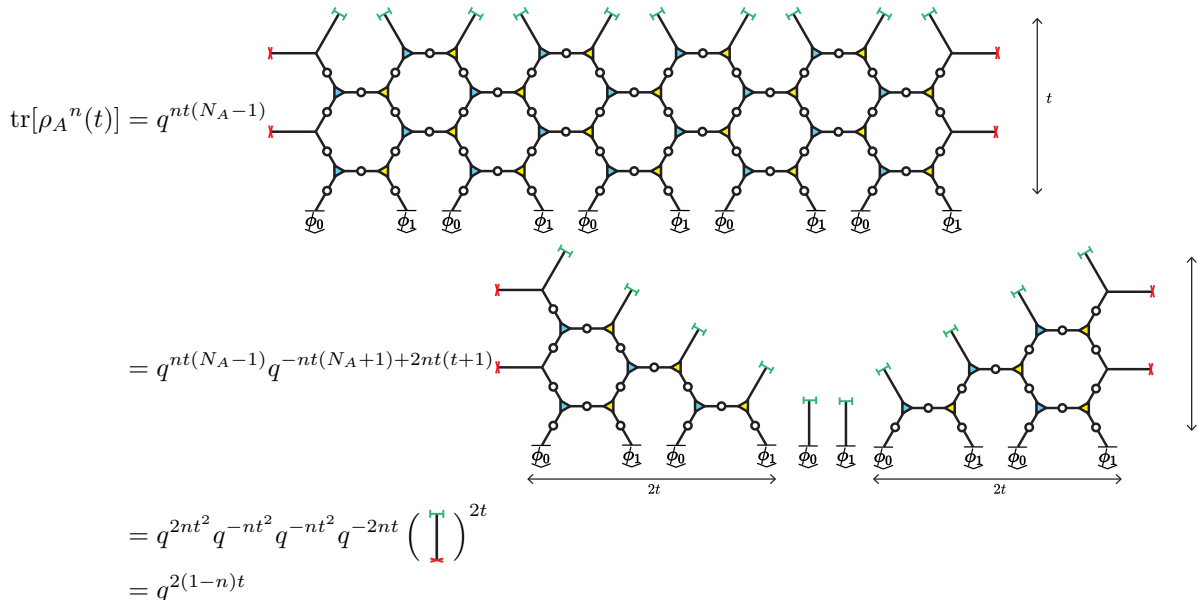
To prove this, we consider  $n$  replicas of the reduced density matrix  $\rho_A$  and calculate the generalized purities  $\text{tr}[\rho_A^n(t)]$ . Then, we take the limit  $\lim_{n \rightarrow 1} S_n$ , where  $S_n$  is the  $n$ -th Rényi entropy  $S_n = \frac{1}{1-n} \log_q \text{tr}[\rho_A^n(t)]$ . To avoid introducing excessive notation, in this section we temporarily generalize the meaning of bold tensors to denote  $n$  replicated pairs of forwards and backwards branches, for example



$$\quad (28)$$

(here depicted for  $n = 3$ ). The third object represents the pairing of the  $n$ -th forward branch of the  $n$  pair with the  $n - 1$ -th backward branch, used in the calculation of the generalized purity.

Then when  $t \leq N_A/4$ , using cancelation of the forwards and backwards branches, we have:



$$\begin{aligned} \text{tr}[\rho_A^n(t)] &= q^{nt(N_A-1)} \\ &= q^{nt(N_A-1)} q^{-nt(N_A+1)+2nt(t+1)} \\ &= q^{2nt^2} q^{-nt^2} q^{-nt^2} q^{-2nt} \left( \text{bold tensor} \right)^{2t} \\ &= q^{2(1-n)t} \end{aligned} \quad (29)$$

where in the first equality we use the unitary condition and in the second equality we use the SIC and triunitary/2DU conditions extensively, while in the third equality we use the following fact:

$$\begin{array}{c} \text{---} \\ | \\ \text{---} \end{array} = q. \quad (30)$$

Thus we have that  $\text{tr}[\rho_A^n(t)] = q^{2(1-n)t}$ , which implies that:

$$S(t) = \lim_{n \rightarrow 1} \frac{1}{1-n} \log_q \text{tr}[\rho_A^n(t)] = 2t, \quad (31)$$

i.e., there is no  $n$ -dependence of the  $n$ -th Rényi entropies  $S_n = \frac{1}{1-n} \log_q \text{tr}[\rho_A^n(t)]$ . From this calculation we note that we have also consequently derived that the entanglement spectrum of  $\rho_A(t)$  (logarithm of the its eigenvalues) is flat (all eigenvalues are either zero or all non-zero but equal in value).

As a technical interlude, while the contraction of the tensor network proceeded straightforwardly enough, we see that the most tricky part of the calculation is keeping track of the coefficients (factors of  $q$ ) that emerge upon simplification of different structures in the TN to factors of the basic diagram  $\begin{array}{c} \text{---} \\ | \\ \text{---} \end{array}$ .

We observe we can instead employ the following trick: we note all local rules of contraction hold true replacing green caps with red crosses, thus giving rise to the exact same coefficients during the intermediate steps. In the latter scenario however, we are calculating  $\text{tr}[\rho_A(t)]^n$ , which we know equals 1. Thus if we denote the coefficient of the final answer as  $C(N_A, n, t)$ , we have:

$$\text{tr}[\rho_A^n(t)] = C(N_A, n, t) \left( \begin{array}{c} \text{---} \\ | \\ \text{---} \end{array} \right)^{2t}, \quad \text{tr}[\rho_A(t)]^n = C(N_A, n, t) \left( \begin{array}{c} \text{---} \\ | \\ \text{---} \end{array} \right)^{2t} = C(N_A, n, t) q^{2nt} = 1. \quad (32)$$

This allows us to easily ascertain  $C(N_A, n, t) = q^{-2nt}$ . We will take this approach in the following sections regarding the replicated version of diagrams. In other words, this trick is nothing more than computing the tensor network of an unnormalized  $\rho_A$ , and then dividing by the normalization factor at the end of the day.

## V. EXACT ENTANGLEMENT DYNAMICS OF THE AKIM WITH $\vec{g}_0 = \vec{0}$ AND ARBITRARY $\vec{g}_1$

Here, we concentrate on the dynamics for the AKIM  $\vec{g}_0 = \vec{0}$  and generic  $\vec{g}_1$  (recall by reflection symmetry all statements hold true upon swapping  $\vec{g}_0$  with  $\vec{g}_1$ ). The same analysis also applies for  $\vec{g}_0$  having components which are  $\pi$  in value. Since we already demonstrated in the previous section all SIC states have exact linear ramps in their entanglement dynamics for early times  $0 \leq t \leq N_A/4$ , we concentrate on the times beyond this.

To begin, we note that when  $\vec{g}_0 = \vec{0}$ , the following local TN identities in the folded representation hold:

$$\begin{array}{c} \circ \\ \diagup \\ \circ \\ \diagdown \\ \circ \end{array} = \begin{array}{c} \circ \\ \diagup \\ \circ \\ \diagdown \\ \circ \end{array}, \quad \begin{array}{c} \circ \\ \diagup \\ \circ \\ \diagdown \\ \circ \end{array} = \frac{1}{q^2} \begin{array}{c} \diagup \\ \diagdown \end{array}, \quad \begin{array}{c} \circ \\ \diagup \\ \circ \\ \diagdown \\ \circ \end{array} = \frac{1}{q} \begin{array}{c} \diagup \\ \diagdown \end{array} \quad (33)$$

When  $\vec{g}_0$  has components containing  $\pi$ , e.g., for qubits  $g_0 = \pi$ , then identical looking diagrammatic identities hold:

$$\begin{array}{c} \circ \\ \diagup \\ \circ \\ \diagdown \\ \circ \end{array} = \begin{array}{c} \circ \\ \diagup \\ \circ \\ \diagdown \\ \circ \end{array}, \quad \begin{array}{c} \circ \\ \diagup \\ \circ \\ \diagdown \\ \circ \end{array} = \frac{1}{q^2} \begin{array}{c} \diagup \\ \diagdown \end{array}. \quad (34)$$

We thus only consider the  $\vec{g}_0$  case in what follows, for simplicity. Again, our strategy will be to compute the generalized purities  $\text{tr}[\rho_A^n(t)]$  and take the limit of the Rényi entropies  $S_n(t)$  as  $n \rightarrow 1$ . As before, we let bold tensors denote  $n$ -copy replicas of the basic tensors, as in Eq. (28).

### A. Late time thermalization

We first establish that for *any* state, the system reaches the infinite temperature state when  $t \geq N_A$  (“late-times”). This amounts to showing that the channel  $\mathcal{C}$ , when raised to the  $N_A$ -th power, becomes a rank-one projector onto

the identity operator. In other words, we desire to show  $\mathcal{C}^{N_A} = q^{-N_A}|I\rangle\rangle\langle\langle I|$ , where  $|I\rangle\rangle$  is the vectorized identity operator. Utilizing Eq. (33) extensively, we compute:

The diagram shows a sequence of three diagrams representing the contraction of  $\mathcal{C}^{N_A}$ . The first diagram is a large hexagonal lattice with red 'X' marks on its boundary edges. The second diagram shows the same lattice with some internal edges highlighted in yellow. The third diagram shows the lattice with a different internal structure. Below these, the lattice is further simplified into a chain of nodes with red 'X' marks, and finally into four vertical lines with red 'X' marks at the top and bottom, representing the identity operator. The entire sequence is labeled with  $\propto$  and  $=$  signs.

where we have utilized the triunitary/2DU properties to simplify the contractions from the third diagram onwards. Mathematically, this implies that  $\mathcal{C}$  has a Jordan block of at most  $N_A$  size.

Nevertheless, as stated in the main text, there is an entire family of dimerized initial states which can achieve earlier thermalization to the infinite-temperature state, which we call the ‘‘maximum-entanglement-solvable states’’. Concretely, if we impose that the initial product state on  $A$  satisfies the SIC as well as the SEC, it will achieve  $S(t) = N_A$  at  $t \geq N_A/2$ . The SEC additionally demands that the initial states  $|\phi_0\rangle|\phi_1\rangle$  satisfy:

The diagram shows two nodes connected by a horizontal line. Each node has two legs extending downwards, labeled  $\phi_0$  and  $\phi_1$ . Red 'X' marks are placed on the top legs of both nodes. The diagram is labeled with an equals sign and the equation number (36).

Let us understand what these solutions are. Writing the additional condition (36) out in unfolded TN, we have:

The diagram shows two unfolded tensor network diagrams connected by an equals sign. Each diagram consists of a central hexagonal lattice with legs extending outwards. The top legs are labeled  $\widehat{\phi}_0^i$  and  $\widehat{\phi}_1^i$ , and the bottom legs are labeled  $\phi_0$  and  $\phi_1$ . Red 'X' marks are placed on the top legs. The diagram is labeled with the equation number (37).

Solving (37) using the results from (24), we have:

$$\begin{array}{c} \widehat{\phi}_0^\dagger \\ | \circ \\ \square^i \text{---} |k\rangle \\ | \circ \\ \widehat{\phi}_1^\dagger \end{array} = 0, \quad i, j, k = 0, 1, \dots, q-1, j \neq k$$

$$\begin{array}{c} \square^i \text{---} |j\rangle^\dagger |j\rangle \\ | \circ \\ \phi_0 \\ | \circ \\ \phi_1 \end{array}$$
(38)

Writing it out explicitly, we have:

$$\langle \phi_0 | -i - k \rangle \langle -i - j | \phi_0 \rangle \langle \phi_1 | H^\dagger | k \rangle \langle j | H | \phi_1 \rangle = 0 \quad (39)$$

where  $| -i - k \rangle := | -i - k \pmod{q} \rangle$ . For qubit case, (39) will reduced to:

$$\langle \phi_0 | 0 \rangle \langle 1 | \phi_0 \rangle \langle \phi_1 | H^\dagger | 0 \rangle \langle 1 | H | \phi_1 \rangle = 0 \quad (40)$$

Here, we define:

$$|z^\perp; \vec{h}\rangle := P(\vec{h})H|0\rangle \quad (41)$$

$$|x^\perp; \vec{h}\rangle := HP(\vec{h})H|0\rangle \quad (42)$$

From construction, we know that  $\langle z^\perp; \vec{h} | Z | z^\perp; \vec{h} \rangle = 0$  and  $\langle x^\perp; \vec{h} | X | x^\perp; \vec{h} \rangle = 0$ . For simplicity of expression, when  $\vec{h}$  is not specified, we denote  $|z^\perp; \vec{h}\rangle$  and  $|x^\perp; \vec{h}\rangle$  as  $|z^\perp\rangle$  and  $|x^\perp\rangle$ . For qubit case, we can prove that the exhaustive set of  $|\phi_0\rangle \otimes |\phi_1\rangle$  satisfying the SEC is  $\{|z\rangle \otimes |x^\perp\rangle\} \cup \{|z^\perp\rangle \otimes |x\rangle\}$ . For qudit in generic dimension, we can verify the set  $\{|z\rangle \otimes |x^\perp\rangle\} \cup \{|z^\perp\rangle \otimes |x\rangle\}$  satisfies the SEC, where  $|x\rangle := H|z\rangle$ .

For this class of states, we then have:

$$\begin{array}{l} \rho_A(t = N_A) \propto \\ \propto \\ \propto \end{array}$$
(43)

as claimed. In going from the second to the third diagram, we ‘opened’ up the diagram starting from the bottom right owing to unitarity in the north-west direction.



### B. Thermalizing dynamics of maximum-entanglement-solvable states for intermediate times

Now we show that the maximum-entanglement-solvable states's full dynamics can be analytically computed for *all* times. Since we have already shown this for early-times  $0 \leq t \leq N_A/4$  and late times  $t \geq N_A$ , we focus on the intermediate times  $N_A/4 < t < N_A$ .

The generalized purity is given by:

$$\begin{aligned}
 \text{tr}[\rho_A^n(t)] &\propto \text{Diagram 1} \propto \text{Diagram 2} \\
 &= \text{Diagram 3} = \text{Diagram 4} \\
 &\propto \text{Diagram 5} \tag{44}
 \end{aligned}$$

Going from the first diagram to the fourth utilizes Eq. (33). In particular, in going from the second to the third, we have added red crosses to the states and also removed a red cross on the top left. From the third to fourth diagram we have removed all red crosses in the bulk, which allows us to cancel many of the gates due to unitarity.

Now since

$$\begin{aligned}
 \text{---} \times |z\rangle &= \text{---} |z\rangle, & \text{---} \times |z^\perp; \vec{h}\rangle &= q^{-n} \text{---} \times
 \end{aligned} \tag{45}$$

we can verify that the set of maximum-entanglement-solvable states  $\{|z\rangle \otimes |x^\perp\rangle\} \cup \{|z^\perp\rangle \otimes |x\rangle\}$  satisfies:

$$\begin{aligned}
 \text{Diagram 6} &= q^{-3n} \text{Diagram 7}, \tag{46}
 \end{aligned}$$

allowing us to contract the TN further so that the generalized purity ultimately takes the form:

$$\begin{aligned}
 \text{tr}[\rho_A^n(t)] &\propto \text{Diagram 8} \propto \left( \text{Diagram 9} \right)^{N_A/2-t} \left( \text{Diagram 10} \right)^{4t-N_A+N_A/2-t} \tag{47}
 \end{aligned}$$

Again, for the maximum-entanglement-solvable states,  $\{|z\rangle \otimes |x^\perp\rangle\} \cup \{|z^\perp\rangle \otimes |x\rangle\}$ , we can verify that

$$\begin{array}{c} \begin{array}{|c|} \hline \mathbb{I} \\ \hline \end{array} \\ \oplus \\ \begin{array}{|c|} \hline \mathbb{I} \\ \hline \end{array} \end{array} = q^{-n} \begin{array}{|c|} \hline \mathbb{I} \\ \hline \end{array} \quad (48)$$

which finally allows us to declare

$$\text{tr}[\rho_A^n(t)] \propto \left( \begin{array}{|c|} \hline \mathbb{I} \\ \hline \end{array} \right)^{2t} \quad (49)$$

From the argument at the end of Sec. IV regarding the appropriate normalization, we thus have that  $\text{tr}[\rho_A^n(t)] = q^{2(1-n)t}$  and

$$S(t) = \lim_{n \rightarrow 1} \frac{1}{1-n} \log_q \text{tr}[\rho_A^n(t)] = \lim_{n \rightarrow 1} \frac{1}{1-n} \log_q q^{2(1-n)t} = 2t \quad (50)$$

## VI. ENTANGLEMENT DYNAMICS OF AKIM AT $(g_0, g_1) = ((2n+1)\pi/2, (2m+1)\pi/2)$

In this section, we focus on qubit systems, and on the AKIM at parameters  $g_0 = (2n+1)\pi/2, g_1 = (2m+1)\pi/2$  where  $n, m \in \mathbb{Z}$ , as was considered in the main text. We note all analyses can be extended to the case of qudits with necessary changes.

We first make a preliminary analysis reducing all analyses down to the single case of  $g_0 = \pi/2, g_1 = \pi/2$ . First, dynamics of the AKIM at these parameter points are all Clifford [4]. This implies that the circuit  $U^t$  at one set of parameters is equal to another, up to some string of Pauli operators. Second, it can be easily verified the dimerized states fulfilling SICs are identical for all parameters  $g_0 = (2n+1)\pi/2, g_1 = (2m+1)\pi/2$ . Combined, this means that the channels  $\mathcal{C}$  governing local dynamics on  $A$  are also related to one another by the action of only an additional Pauli channel. Immediately this implies entanglement dynamics of the AKIM is identical in this family of parameters (as long as we prepare the same state), and so we can focus on the case  $(g_0, g_1) = (\pi/2, \pi/2)$ .

However, if we are interested in the reduced density matrices themselves, we have to understand the channels themselves. It is straightforward to work out the following relations between them. Let  $\mathcal{C}_{1(3)/2, 1(3)/2}$  denote the channel of the AKIM at the parameters  $(g_0, g_1) = (1(3) \times \pi/2, 1(3) \times \pi/2)$ . Then we can easily check that:

$$\begin{aligned} \mathcal{P}_{IYIY\dots} \circ \mathcal{C}_{1/2, 1/2}^t &= \mathcal{C}_{1/2, 3/2}^t \text{ for } t = 4n + 1, n \in \mathbb{N} \\ \mathcal{P}_{YIYI\dots} \circ \mathcal{C}_{1/2, 1/2}^t &= \mathcal{C}_{1/2, 3/2}^t \text{ for } t = 4n + 2, n \in \mathbb{N} \\ \mathcal{P}_{YIYI\dots} \circ \mathcal{C}_{1/2, 1/2}^t &= \mathcal{C}_{1/2, 3/2}^t \text{ for } t = 4n + 3, n \in \mathbb{N} \\ \mathcal{C}_{1/2, 1/2}^t &= \mathcal{C}_{1/2, 3/2}^t \text{ for } t = 4n + 4, n \in \mathbb{N}, \end{aligned} \quad (51)$$

where  $\mathcal{P}_P[\rho] = \frac{1}{2}(\rho + P\rho P^\dagger)$  for a Pauli string  $P$ ; and

$$\begin{aligned} \mathcal{P}_{YIYI\dots} \circ \mathcal{C}_{1/2, 1/2}^t &= \mathcal{C}_{3/2, 3/2}^t \text{ for } t = 2n + 1, n \in \mathbb{N} \\ \mathcal{C}_{1/2, 1/2}^t &= \mathcal{C}_{3/2, 3/2}^t \text{ for } t = 2n + 2, n \in \mathbb{N}. \end{aligned} \quad (52)$$

This will allow us to focus on only the case of  $(g_0, g_1) = (\pi/2, \pi/2)$ , whereupon we can translate all results from there to other cases, with consideration of the action of the additional Pauli channel.

Let us state a summary of our findings:

- As argued above, entanglement dynamics of a given state is the same for any parameter values of the AKIM of the form  $((2n+1)\pi/2, (2m+1)\pi/2)$ .
- For  $(g_0, g_1) = (\pi/2, \pi/2)$ ,  $\mathcal{C}_{1/2, 1/2}^{N_A/2+1} = \mathcal{C}_{1/2, 1/2}^{N_A/2+2}$ . This implies the system always equilibrates regardless of initial state at time  $t = N_A/2 + 1$ .
- However, there are multiple steady states — the equilibrium state is not unique. This is because of the existence of an exponential (i.e., super-extensive!) set of conserved quantities:  $2^{N_A-1}$  operators consisting of independent products of  $Z_i Z_{i+1}$  on odd bonds and  $X_i X_{i+1}$  on even bonds.

- For  $(g_0, g_1) = (3\pi/2, 3\pi/2)$ , we also have  $\mathcal{C}_{3/2,3/2}^{N_A/2+1} = \mathcal{C}_{3/2,3/2}^{N_A/2+2}$ , i.e., equilibration regardless of initial state at  $t = N_A/2 + 1$ . This is because the channel  $\mathcal{P}_{Y\bar{Y}Y\bar{Y}\dots}$  acts trivially on the conserved quantities of  $(g_0, g_1) = (\pi/2, \pi/2)$ , so that  $\mathcal{C}_{3/2,3/2}^t = \mathcal{C}_{1/2,1/2}^t$  for  $t \geq N_A/2 + 1$ .
- For  $(g_0, g_1) = (\pi/2, 3\pi/2)$  the situation is more interesting. It can be seen  $\mathcal{P}_{I\bar{Y}I\bar{Y}\dots}$  has the same action as  $\mathcal{P}_{Y\bar{Y}Y\bar{Y}\dots}$  on the conserved quantities which is non-trivial (some operators pick up under a minus sign under this channel, for example  $Z_1 Z_2$ ). Thus, for  $t \geq N_A/2 + 1$ , we have  $\mathcal{C}_{1/2,3/2}^t = \mathcal{P}_{I\bar{Y}I\bar{Y}} \circ \mathcal{C}_{1/2,1/2}^t$  for  $t = 2n + 1, n \in \mathbb{N}$  and  $\mathcal{C}_{1/2,3/2}^t = \mathcal{C}_{1/2,1/2}^t$  for  $t = 2n + 2, n \in \mathbb{N}$ , i.e., the system oscillates between two ‘steady’-states.

Let us now prove these statements. When  $g_0 = g_1 = \frac{\pi}{2}$ , we identify the following local TN contraction rules:

$$\text{Diagrammatic equation (53)} \quad (53)$$

$$\text{Diagrammatic equation (54)} \quad (54)$$

$$\text{Diagrammatic equation (55)} \quad (55)$$

Note in the last figure, there is an avoided crossing of lines. We will use Eqs. (53) and (54) extensively in the following calculation for finite-time entanglement saturation, where Eq. (53) serves as the rule describing the emergence of red cross tensors in the bulk of the subsystem, and Eq. (54) is the useful diagrammatic tool for reduction of the TN. We will use Eq. (55) in the computation of entanglement dynamics.

### A. Exact finite time entanglement saturation

We claim that the quantum channel  $\mathcal{C}$  for subsystem  $A$  has the following property:

$$\mathcal{C}^{N_A/2+k} = \mathcal{C}^{N_A/2+1}, \quad \forall k \in \mathbb{N}^+. \quad (56)$$

To prove this property we first derive the diagrammatic expression for  $\mathcal{C}^{N_A/2+1}$ :

$$\mathcal{C}^{N_A/2+1} \propto \text{Diagrammatic expression for } \mathcal{C}^{N_A/2+1} \quad (57)$$

$$\propto \propto \propto \quad (57)$$

where we have used the previously quoted local TN identities and also used the first equation of Eq. (33). Since unitality enforces  $\mathcal{C}^{N_A/2+1}[I] = I$ , this fixes the normalization constant:

$$\mathcal{C}^{N_A/2+1} = 2^{N_A-1} \propto \quad (58)$$

Next we prove that  $\mathcal{C}^{N_A/2+2} = \mathcal{C}^{N_A/2+1}$ . We notice:

$$\mathcal{C}^{N_A/2+2} \propto \propto \propto \propto \quad (59)$$

By unitality this fixes the normalization constant again so that  $\mathcal{C}^{N_A/2+2} = \mathcal{C}^{N_A/2+1}$  and we can then complete the proof of Eq. (56) by induction.

It is instructive to understand physically the action of the late-time channel  $\mathcal{C}^{N_A/2+1}$ . From the folded TN representation of  $\mathcal{C}^{N_A/2+1}$ , we notice that it is a composition of three local channels:

$$c = 2 \propto, \quad c[\rho] = \frac{1}{2}(\rho + (X \otimes X)\rho(X \otimes X)) \quad (60)$$

$$d = 2 \propto, \quad d[\rho] = \frac{1}{2}(\rho + (Z \otimes Z)\rho(Z \otimes Z)) \quad (61)$$

$$b = \propto, \quad b[\rho] = \frac{1}{2}(\rho + Z\rho Z) \quad (62)$$

Then we have:

$$\mathcal{C}^{N_A/2+1} = b_1 \circ b_{N_A} \circ \prod_{\text{even bonds}} d \circ \prod_{\text{odd bonds}} c \quad (63)$$

In other words, the late-time channel describes  $XX$  dissipation on odd bonds followed by  $ZZ$  dissipation on even bonds, and lastly  $Z$ -dephasing on the boundaries.

We can fully understand the spectral decomposition of the late-time channel  $\mathcal{C}^{N_A/2+1}$ . Since it is the composition of local channels which are all Pauli channels, its eigenvectors are all Pauli strings, and its eigenvalues are 1 or 0. Precisely, the set of Pauli strings that commutes with all of the Kraus operators of the local channels are the eigenvectors with unity eigenvalues, and are hence conserved quantities in dynamics, while the set of Pauli strings which commutes with at least one Kraus operator are the eigenvectors with zero eigenvalues. The former set is exhausted by all independent products of  $ZZ$  operators on odd bonds and  $XX$  operators on even bonds, of which there are  $2^{N_A-1}$  of them. For example, for  $N_A = 4$ , we have 8 operators  $IIII, ZZII, IIZZ, IXXI, ZYXI, IXYZ, ZYYZ, ZZZZ$ .

### B. Exact entanglement dynamics with maximal saturation of entropy

Although there are super-extensive conserved quantities for the case of  $g_0 = g_1 = \pi/2$ , we can still achieve thermalization to infinite temperature with exact linear growth of entanglement for some specific states. Here we prove that for the large family of dimerized product states  $|z\rangle \otimes |z^\perp\rangle$  and  $|y\rangle \otimes |x^\perp\rangle$ , they have linear entanglement growth with slope 2 and reach the infinite-temperature state when  $t \geq N_A/2$ . In other words,

$$S(t) = \min(2t, N_A). \quad (64)$$

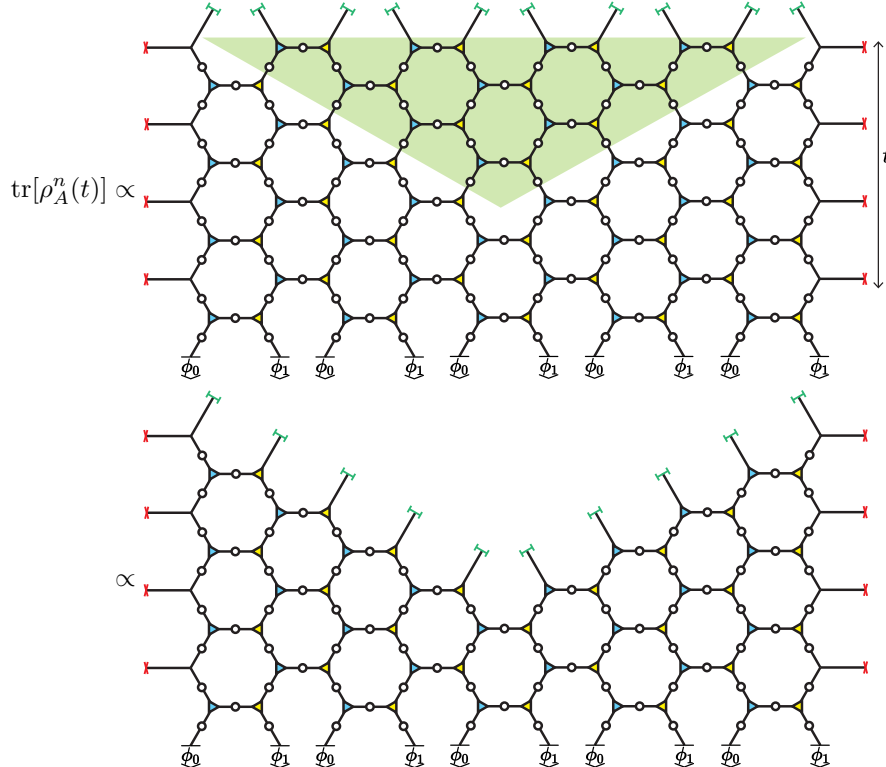
Note that by symmetry, this holds true for  $|z^\perp\rangle \otimes |z\rangle$  and  $|y^\perp\rangle \otimes |x\rangle$  too. We dub these the “maximum-entanglement-solvable” states.

We take the following approach. First, we will prove that for  $t \leq N_A/2$ , we have  $\text{tr}[\rho_A^n(t)] = 2^{2t(1-n)}$  and thus  $S(t) = 2t$ . This then implies  $\rho_A(N_A/2) \propto I_A$  as it is the unique state with maximal entropy, which is then seen to be a steady-state for times  $t \geq N_A/2$ . For the calculation, we will use the following fact extensively:

$$\begin{array}{c} \text{---} \text{---} \text{---} \\ | \\ \text{---} \end{array} = \frac{1}{q} \text{---} \text{---} \quad (65)$$

to break up the TN diagram. We note an analogous relation holds upon changing a green end into a red cross (they just represent different pairings of forwards and backwards branches of the  $n$  replicas).

To begin, we observe  $|z\rangle \otimes |z^\perp\rangle$  and  $|y\rangle \otimes |x^\perp\rangle$  satisfy the SIC, so they achieve exact linear entanglement growth for  $t \leq N_A/4$  as we proved in Sec. IV. For intermediate times  $N_A/4 \leq t \leq N_A/2$  we have the following diagram, which we can contract:



$$\begin{aligned}
& \propto \\
& = \\
& = \\
& \propto \langle L_1 | \quad T_l \quad T_m \quad T_r \quad | R_1 \rangle \\
& = \langle L_1 | T_l^{N_A/2-t} T_m^{2t-N_A/2-1} T_r^{N_A/2-t} | R_1 \rangle
\end{aligned} \tag{66}$$

Above,  $l$  stands for left;  $m$  for middle; and  $r$  for right. Going from the first line to the second, we canceled gates within the causal light-cone away from the boundaries (green triangle); from the second to third, we used Eqs. (53) and (54); in moving to the fourth, fifth and sixth line we used (55) repeatedly.

The end result, Eq. (66), is an elucidation of the general, simplified structure of the generalized purity in the intermediate time regime: it is a 1D diagram consisting of contraction of boundary states  $\langle L_1, |R_1\rangle$  within bulk tensors  $T_l, T_m, T_r$  of varying numbers depending on system size  $N_A$  and time  $t$ .

Now we contract the 1D TN, Eq. (66), for the states  $|\phi_0\rangle \otimes |\phi_1\rangle = |z\rangle \otimes |z^\perp\rangle$ . We have

$$\langle L_1 | T_l = \text{[Diagram]} = \text{[Diagram]} \propto \text{[Diagram]} \tag{67}$$

$$\propto \begin{array}{c} \color{red}{\text{I}} \\ \color{red}{\text{I}} \\ \color{red}{\text{I}} \end{array} \propto \begin{array}{c} \color{red}{\text{I}} \\ \color{red}{\text{I}} \\ \color{red}{\text{I}} \end{array} \propto \begin{array}{c} \color{red}{\text{I}} \\ \color{red}{\text{I}} \\ \color{red}{\text{I}} \end{array} \quad (68)$$

where for the second equality, we used the results from the first equalities of Eq. (45) and Eq. (53); and for the first proportionality we used the two equalities of Eq. (45) since  $H|z\rangle \in \{|z^\perp\rangle\}$ . Next define

$$\langle L_2| := \begin{array}{c} \color{red}{\text{I}} \\ \color{red}{\text{I}} \\ \color{red}{\text{I}} \end{array} \quad (69)$$

We will see this same structure is preserved as we perform contraction of the 1D TN Eq. (66) going from left to right, with factors  $\begin{array}{c} \color{red}{\text{I}} \\ \color{red}{\text{I}} \\ \color{red}{\text{I}} \end{array}$  'popping' out.

Indeed, applying  $\langle L_2|$  with  $T_l$  we have

$$\langle L_2|T_l = \begin{array}{c} \color{red}{\text{I}} \\ \color{red}{\text{I}} \\ \color{red}{\text{I}} \end{array} \propto \begin{array}{c} \color{red}{\text{I}} \\ \color{red}{\text{I}} \\ \color{red}{\text{I}} \end{array} \propto \begin{array}{c} \color{red}{\text{I}} \\ \color{red}{\text{I}} \\ \color{red}{\text{I}} \end{array} = \begin{array}{c} \color{red}{\text{I}} \\ \color{red}{\text{I}} \\ \color{red}{\text{I}} \end{array} \langle L_2|, \quad (70)$$

while for  $T_m$ ,

$$\langle L_2|T_m = \begin{array}{c} \color{red}{\text{I}} \\ \color{red}{\text{I}} \\ \color{red}{\text{I}} \end{array} \propto \begin{array}{c} \color{red}{\text{I}} \\ \color{red}{\text{I}} \\ \color{red}{\text{I}} \end{array} \propto \begin{array}{c} \color{red}{\text{I}} \\ \color{red}{\text{I}} \\ \color{red}{\text{I}} \end{array} \propto \begin{array}{c} \color{red}{\text{I}} \\ \color{red}{\text{I}} \\ \color{red}{\text{I}} \end{array} \propto \begin{array}{c} \color{red}{\text{I}} \\ \color{red}{\text{I}} \\ \color{red}{\text{I}} \end{array} = \left( \begin{array}{c} \color{red}{\text{I}} \\ \color{red}{\text{I}} \\ \color{red}{\text{I}} \end{array} \right)^2 \langle L_2|. \quad (71)$$

For  $T_r$ ,

$$\langle L_2|T_r = \begin{array}{c} \color{red}{\text{I}} \\ \color{red}{\text{I}} \\ \color{red}{\text{I}} \end{array} \propto \begin{array}{c} \color{red}{\text{I}} \\ \color{red}{\text{I}} \\ \color{red}{\text{I}} \end{array} \propto \begin{array}{c} \color{red}{\text{I}} \\ \color{red}{\text{I}} \\ \color{red}{\text{I}} \end{array} \propto \begin{array}{c} \color{red}{\text{I}} \\ \color{red}{\text{I}} \\ \color{red}{\text{I}} \end{array} = \begin{array}{c} \color{red}{\text{I}} \\ \color{red}{\text{I}} \\ \color{red}{\text{I}} \end{array} \langle L_2|. \quad (72)$$

Lastly, we take the overlap of  $\langle L_2|$  with the right boundary state  $|R_1\rangle$ .

$$\langle L_2|R_1 = \begin{array}{c} \color{red}{\text{I}} \\ \color{red}{\text{I}} \\ \color{red}{\text{I}} \end{array} \propto \begin{array}{c} \color{red}{\text{I}} \\ \color{red}{\text{I}} \\ \color{red}{\text{I}} \end{array} \propto \begin{array}{c} \color{red}{\text{I}} \\ \color{red}{\text{I}} \\ \color{red}{\text{I}} \end{array} = \begin{array}{c} \color{red}{\text{I}} \\ \color{red}{\text{I}} \\ \color{red}{\text{I}} \end{array} \quad (73)$$

So if  $N_A/2 \leq t < N_A/2$ , we can see  $\text{tr}[\rho_A^n(t)] \propto \left( \begin{array}{c} \color{red}{\text{I}} \\ \color{red}{\text{I}} \\ \color{red}{\text{I}} \end{array} \right)^{2t}$ . For the special case of  $t = N_A/2$ , we instead have:

$$\text{tr}[\rho_A^n(N_A/2)] = \langle L_1|T_m^{N_A/2-1}|R_1\rangle. \quad (74)$$

Now since

$$\langle L_1|T_m = \begin{array}{c} \color{red}{\text{I}} \\ \color{red}{\text{I}} \\ \color{red}{\text{I}} \end{array} \propto \begin{array}{c} \color{red}{\text{I}} \\ \color{red}{\text{I}} \\ \color{red}{\text{I}} \end{array} \propto \begin{array}{c} \color{red}{\text{I}} \\ \color{red}{\text{I}} \\ \color{red}{\text{I}} \end{array} \quad (75)$$

$$= \begin{array}{c} \color{red}{\text{I}} \\ \color{red}{\text{I}} \\ \color{red}{\text{I}} \end{array} \propto \begin{array}{c} \color{red}{\text{I}} \\ \color{red}{\text{I}} \\ \color{red}{\text{I}} \end{array} \propto \begin{array}{c} \color{red}{\text{I}} \\ \color{red}{\text{I}} \\ \color{red}{\text{I}} \end{array} = \left( \begin{array}{c} \color{red}{\text{I}} \\ \color{red}{\text{I}} \\ \color{red}{\text{I}} \end{array} \right)^2 \langle L_1|, \quad (76)$$

and

$$\langle L_1|R_1 = \begin{array}{c} \color{red}{\text{I}} \\ \color{red}{\text{I}} \\ \color{red}{\text{I}} \end{array} = \begin{array}{c} \color{red}{\text{I}} \\ \color{red}{\text{I}} \\ \color{red}{\text{I}} \end{array} \propto \begin{array}{c} \color{red}{\text{I}} \\ \color{red}{\text{I}} \\ \color{red}{\text{I}} \end{array} \propto \begin{array}{c} \color{red}{\text{I}} \\ \color{red}{\text{I}} \\ \color{red}{\text{I}} \end{array} = \left( \begin{array}{c} \color{red}{\text{I}} \\ \color{red}{\text{I}} \\ \color{red}{\text{I}} \end{array} \right)^2, \quad (77)$$

therefore

$$\text{tr}[\rho_A^n(N_A/2)] \propto \left( \prod_{i=1}^n \mathbb{I} \right)^{N_A} \implies \text{tr}[\rho_A^n(N_A/2)] = 2^{N_A(1-n)}. \quad (78)$$

Conversely for  $|\phi_0\rangle \otimes |\phi_1\rangle = |y\rangle \otimes |x^\perp\rangle$ , we notice that

$$\langle L_1 | T_l = \begin{array}{c} \text{Diagram 1} \\ \text{Diagram 2} \\ \text{Diagram 3} \\ \text{Diagram 4} \end{array} \quad (79)$$

$$\langle L_1 | T_m = \begin{array}{c} \text{Diagram 5} \\ \text{Diagram 6} \end{array} \quad (80)$$

$$\propto \begin{array}{c} \text{Diagram 7} \\ \text{Diagram 8} \\ \text{Diagram 9} \end{array} \quad (81)$$

$$\text{Tr} | R_1 \rangle = \begin{array}{c} \text{Diagram 10} \\ \text{Diagram 11} \\ \text{Diagram 12} \\ \text{Diagram 13} \end{array} \propto \mathbb{I} | R_1 \rangle \quad (82)$$

$$\langle L_1 | R_1 \rangle = \begin{array}{c} \text{Diagram 14} \\ \text{Diagram 15} \\ \text{Diagram 16} \end{array} \propto \left( \prod_{i=1}^n \mathbb{I} \right)^2 \quad (83)$$

Thus for  $t \leq N_A/2$ ,  $\text{tr}[\rho_A^n(t)] \propto \left( \prod_{i=1}^n \mathbb{I} \right)^{2t}$  in both scenarios, which implies  $\text{tr}[\rho_A^n(t)] = 2^{2t(1-n)}$  and hence  $S_n(t) = 2t$ . Upon taking the analytic continuation  $n \rightarrow 1$  of the  $n$ -th Rényi entropies we thus obtain our claimed result for the von Neumann entropy  $S(t)$ .

### C. Exact entanglement dynamics with non-maximal saturation of entropy

Here we demonstrate a state for which exact entanglement dynamics can be computed, though saturation of entropy is non-maximal. Specifically we prove that for  $|\phi_0\rangle \otimes |\phi_1\rangle = |z\rangle \otimes |z\rangle$ , we have

$$S(t) = \min\{2t, N_A/2\}. \quad (84)$$

(Recall  $t \in \mathbb{N}$ ).

We first notice that  $|z\rangle \otimes |z\rangle$  satisfies the SIC condition, which means that we already have exact linear growth of entanglement dynamics when  $t \leq N_A/4$ , with slope 2. For  $t \geq N_A/2 + 1$ , we have:

$$\begin{array}{c} \text{tr}[\rho_A^n(t)] \propto \text{Diagram 17} \\ \propto \text{Diagram 18} \\ \propto \text{Diagram 19} = \left( \prod_{i=1}^n \mathbb{I} \right)^{N_A/2} \end{array} \quad (85)$$



Then we focus on the regime  $N_A/4 < t \leq N_A/2$ . We have

$$\text{tr}[\rho_A^n(t)] \propto \langle L_1 | T_l^{N_A/2-t} T_m^{2t-N_A/2-1} T_r^{N_A/2-t} | R_1 \rangle, \quad (86)$$

as stated in the former subsection. Since

$$\langle L_1 | T_l = \begin{array}{c} \text{Diagram 1} \\ \text{Diagram 2} \\ \text{Diagram 3} \\ \text{Diagram 4} \\ \text{Diagram 5} \\ \text{Diagram 6} \end{array} \propto \langle L_1 | \quad (87)$$

$$\langle L_1 | T_m = \begin{array}{c} \text{Diagram 7} \\ \text{Diagram 8} \\ \text{Diagram 9} \\ \text{Diagram 10} \end{array} \propto \langle L_1 | \quad (88)$$

Analogous to the calculation for  $\langle L_1 | T_l$ , undergoing contraction from right to left instead of from left to right, we find:

$$T_r | R_1 \rangle = \begin{array}{c} \text{Diagram 11} \\ \text{Diagram 12} \\ \text{Diagram 13} \end{array} \propto | R_1 \rangle. \quad (89)$$

Additionally, we have:

$$\langle L_1 | R_1 \rangle = \begin{array}{c} \text{Diagram 14} \\ \text{Diagram 15} \\ \text{Diagram 16} \\ \text{Diagram 17} \end{array} \propto \langle L_1 |. \quad (90)$$

Thus for  $N_A/4 < t \leq N_A/2$ , we obtain  $\text{tr}[\rho_A^n(t)] \propto \left( \langle L_1 | \right)^{N_A/2}$ , leading to the fact that  $\text{tr}[\rho_A^n(t)] = 2^{(1-n)N_A/2}$ , and upon performing an analytic continuation  $n \rightarrow 1$  our stated claim of  $S(t)$ .

## VII. GAP OF QUANTUM CHANNEL $\mathcal{C}$

In this section, we numerically investigate the channel  $\mathcal{C}$  governing dynamics on  $A$ , Eq. (21). In particular, we compute the gap  $\Delta$  defined as

$$\Delta := 1 - |\lambda| \quad (91)$$

where  $\lambda$  is the eigenvalue of  $\mathcal{C}$  not belonging to the eigenvector which is the identity operator, which physically sets the rate of thermalization. This is shown in Fig. 1 for  $N_A = 4$ . Note the definition of the gap above is a slightly different formulation than the one quoted in the main text.

We see from Fig. 1 that along  $g_0 = 0, \pi$  or  $g_1 = 0, \pi$ ,  $\Delta = 1$ , indicating that the maximally-mixed state  $\mathbb{I}$  is the unique unity eigenvector, and all other eigenvectors carry zero eigenvalues. This implies that thermalization to infinite-temperature is necessarily attained at some finite time. At  $g_0 = g_1 = \pi/2$ ,  $g_0 = \pi/2, g_1 = 3\pi/2$ ,  $g_0 = 3\pi/2, g_1 = \pi/2$ , and  $g_0 = g_1 = 3\pi/2$ , we see  $\Delta = 0$ , indicating the presence of degenerate steady-states or oscillatory non-decaying states. Finally, for generic  $g_0, g_1$  away from these special regions, we see  $0 < \Delta < 1$ , indicating the system has a unique steady-state (the identity operator), and that the approach only is generically attained exponentially quickly (as opposed to exactly at some finite time), with the rate set by the gap  $\Delta$ .

## VIII. TRACKING STABILIZERS AND OPERATOR ENTANGLEMENT

We consider the AKIM on a system of qubits in this section. For the “maximum-entanglement-solvable” states found for  $g_0$  (or for  $g_1 = g_2 = \pi/2$ ), our calculation in Sec. V (and Sec. VI) yielded that the  $n$ -th Rényi entropy of the

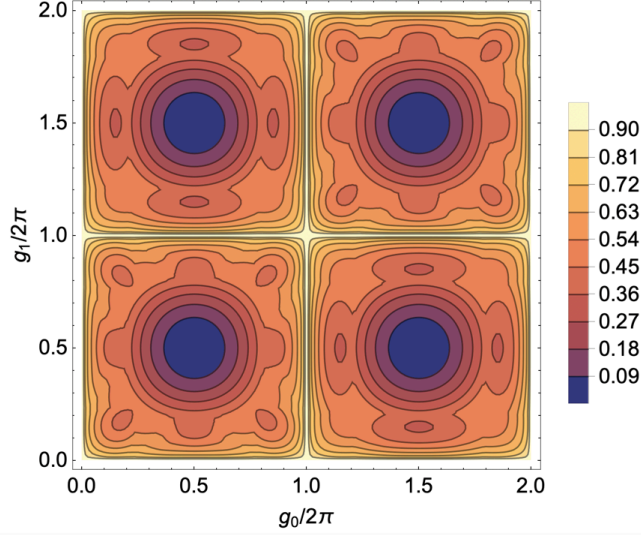


FIG. 1. Gap  $\Delta$  of the channel  $\mathcal{C}$  at different parameters  $(g_0, g_1)$  of the AKIM. We see the gap is 1 along the lines  $g_0 = 0, \pi$  and  $g_1 = 0, \pi$ , while it is 0 at  $g_0 = (2n + 1)\pi/2, g_1 = (2m + 1)\pi/2$ , where  $n, m \in \mathbb{Z}$ .

RDM  $\rho_A(t)$  is  $\min(2t, N_A)$  and in particular independent of  $n$ , indicating that its entanglement spectrum (logarithm of eigenvalues of  $\rho_A(t)$ ) is flat at any time. Thus, we *must* be able to decompose  $\rho_A(t)$  products of projectors

$$\rho_A(t) = \frac{1}{2^{N_A}} \prod_{n=1}^{N_A - \min(2t, N_A)} (1 + O_n^{(t)}) \quad (92)$$

where  $O_n^{(t)}$  are Hermitian operators satisfying  $[O_n^{(t)}, O_m^{(t)}] = 0$  and  $\text{eig}(O_n^{(t)}) = \pm 1$  with equal degeneracies. In other words,  $O_n^{(t)}$  are the *stabilizers* of the RDM at a given time  $t$ . Of course, we note that this decomposition is not unique, as products of stabilizers yield new valid stabilizers; one just has to pick a maximal set of algebraically independent ones.

Our aim here is to investigate the fine-structure of these stabilizers; in particular, their operator entanglement. Concretely, we fix  $N_A = 6, g_0 = 0$ , allow arbitrary  $g_1$ , and consider the initial state on A prepared as a dimerized product state  $|0\rangle \otimes e^{i\theta X} |0\rangle$ .

At time  $t = 0$ , since  $\rho_A(t)$  is a product state, it is easy to write down its stabilizers:

$$\begin{aligned} O_1^{(1)} &= Z_1, \\ O_2^{(1)} &= \cos(2\theta)Z_2 + \sin(2\theta)Y_2, \\ O_3^{(1)} &= Z_3, \\ O_4^{(1)} &= \cos(2\theta)Z_4 + \sin(2\theta)Y_4, \\ O_5^{(1)} &= Z_5, \\ O_6^{(1)} &= \cos(2\theta)Z_6 + \sin(2\theta)Y_6. \end{aligned} \quad (93)$$

At  $t = 1$ , we find

$$\begin{aligned} O_1^{(2)} &= Z_1 X_2 \\ O_2^{(2)} &= Z_3 X_4 \\ O_3^{(2)} &= (\cos(g_1 + 2\theta)X_3 - \sin(g_1 + 2\theta)Y_3)Z_4 \\ O_4^{(2)} &= (\cos(g_1 + 2\theta)X_5 - \sin(g_1 + 2\theta)Y_5)Z_6 \end{aligned} \quad (94)$$

While more complicated than the stabilizers at  $t = 0$  (they are now more non-local), they are all still expressible as a tensor product of local operators  $o_i \otimes o_j$  on sites  $i, j$ , i.e., they do not harbor operator entanglement.

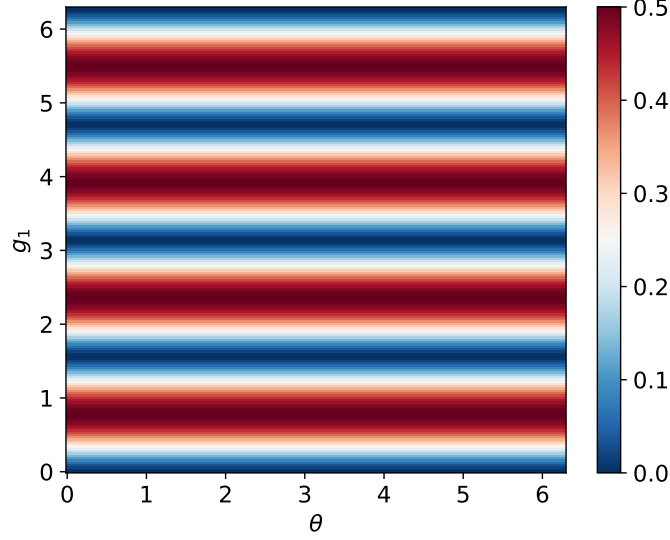


FIG. 2. Operator entanglement entropy of stabilizer  $O^{(2)}$ . Away from the Clifford points  $g_1 = n\pi/2$ , the stabilizer develops a complicated spatial structure, captured by the presence of operator entanglement.

The situation is more interesting when  $t = 2$ . We find

$$\begin{aligned}
O_1^{(2)} &= Z_1 Z_3 X_4, \\
O_2^{(2)} &= s_{g_1} c_{g_1} c_{2(g_1+\theta)} X_3 Y_4 Z_6 - s_{g_1} s_{g_1} s_{2(g_1+\theta)} X_3 Y_4 Z_5 Z_6 + c_{g_1} c_{g_1} c_{2(g_1+\theta)} X_3 Z_4 Z_6 - s_{g_1} c_{g_1} s_{2(g_1+\theta)} X_3 Z_4 Z_5 Z_6 \\
&\quad - s_{g_1} c_{g_1} s_{2(g_1+\theta)} Y_3 Y_4 Z_6 - s_{g_1} s_{g_1} c_{2(g_1+\theta)} Y_3 Y_4 Z_5 Z_6 - c_{g_1} c_{g_1} s_{2(g_1+\theta)} Y_3 Z_4 Z_6 - s_{g_1} c_{g_1} c_{2(g_1+\theta)} Y_3 Z_4 Z_5 Z_6, \quad (95)
\end{aligned}$$

where  $c_x = \cos(x)$  and  $s_x = \sin(x)$ . While  $O_1^{(2)}$  is simple,  $O_2^{(2)}$  appears complicated (furthermore, this complexity is preserved even if we consider their product,  $O_1^{(2)} O_2^{(2)}$ ).

We probe  $O_2^{(2)}$ 's operator entanglement entropy for a bipartition into sites 1 : 3 (L), and sites 4 : 6 (R). This is defined as follows. We write  $O_2^{(2)}$  in its Schmidt decomposition

$$O_2^{(2)} = \sum_i \sqrt{p_i} O_{i,L} \otimes O_{i,R} \quad (96)$$

where  $O_{i,L}, O_{j,L}$  are assumed to be mutually orthonormal under the Hilbert-Schmidt inner product,  $O_{i,R}, O_{j,R}$  are assumed to be mutually orthonormal under the Hilbert-Schmidt inner product, and  $p_i \geq 0$ . The operator entanglement is defined to be the Shannon entropy associated with  $\{p_i\}$ . A simpler and alternative way to understand it is to treat the operators as living in a vector space, so that we can formally map  $I \mapsto |0\rangle, X \mapsto |1\rangle, Y \mapsto |2\rangle, Z \mapsto |3\rangle$  and consider the entanglement entropy of the resulting quantum state. Since  $O_2^{(2)}$  has no support on sites 1, 2 and since it has a common action  $Z_6$  on site 6, the operator entanglement entropy reduces to the bipartite entanglement entropy of the state

$$\begin{aligned}
|\psi\rangle &= s_{g_1} c_{g_1} c_{2(g_1+\theta)} |120\rangle - s_{g_1} s_{g_1} s_{2(g_1+\theta)} |123\rangle + c_{g_1} c_{g_1} c_{2(g_1+\theta)} |130\rangle - s_{g_1} c_{g_1} s_{2(g_1+\theta)} |133\rangle \\
&\quad - s_{g_1} c_{g_1} s_{2(g_1+\theta)} |220\rangle - s_{g_1} s_{g_1} c_{2(g_1+\theta)} |223\rangle - c_{g_1} c_{g_1} s_{2(g_1+\theta)} |230\rangle - s_{g_1} c_{g_1} c_{2(g_1+\theta)} |233\rangle, \quad (97)
\end{aligned}$$

between sites 1 and sites 2,3. We further notice we can factor the state on site 2 as  $s_{g_1}|2\rangle + c_{g_1}|3\rangle$ , leaving a reduced state on sites 1 and 3

$$|\psi'\rangle = c_{g_1} c_{2(g_1+\theta)} |10\rangle - s_{g_1} s_{2(g_1+\theta)} |13\rangle - c_{g_1} s_{2(g_1+\theta)} |20\rangle - s_{g_1} c_{2(g_1+\theta)} |23\rangle. \quad (98)$$

Forming the reduced density matrix on site 1 we get

$$\rho_{\psi'} = (c_{g_1}^2 c_{2(g_1+\theta)}^2 + s_{g_1}^2 s_{2(g_1+\theta)}^2) |1\rangle\langle 1| + (c_{g_1}^2 s_{2(g_1+\theta)}^2 + s_{g_1}^2 c_{2(g_1+\theta)}^2) |2\rangle\langle 2| + (-c_{g_1}^2 + s_{g_1}^2) s_{2(g_1+\theta)} c_{2(g_1+\theta)} (|1\rangle\langle 2| + |2\rangle\langle 1|). \quad (99)$$

Plotting the entanglement entropy of this state (in log base 4) for various  $g_1$  and  $\theta$  yields Fig. 3(a) of the main text, reproduced here in Fig. 2. We see that the stabilizer has non-trivial operator entanglement for any  $g_1 \neq m\pi$ ,  $m \in \mathbb{Z}$ , so dynamics at these points is surely not Clifford, even in some ‘secretly locally-rotated’ basis.

Lastly, at  $t = 3$ , there ceases to be any more stabilizers and the state has thermalized to infinite-temperature:  $\rho_A(t) = I_A/2^{N_A}$ .

- 
- [1] Bruno Bertini, Pavel Kos, and Tomaz Prosen. Localised dynamics in the floquet quantum east model. *arXiv:2306.12467*, January 2022.
  - [2] Bruno Bertini, Cecilia De Fazio, Juan P. Garrahan, and Katja Klobas. Exact quench dynamics of the floquet quantum east model at the deterministic point, 2023.
  - [3] Alessio Lerose, Michael Sonner, and Dmitry A. Abanin. Influence matrix approach to many-body floquet dynamics. *Phys. Rev. X*, 11:021040, May 2021.
  - [4] Michael A. Nielsen and Isaac L. Chuang. *Quantum Computation and Quantum Information*. Cambridge University Press, Cambridge, 2000.